Density functional theory studies of the structural, electronic, and phonon properties of Li_2O and Li_2CO_3: Application to CO_2 capture reaction

Yuhua Duan[1,2,*] and Dan C. Sorescu[1]

[1]*National Energy Technology Laboratory, United States Department of Energy, Pittsburgh, Pennsylvania 15236, USA*

[2]*Parsons Corporation, South Park, Pennsylvania 15129, USA*

(Received 21 August 2008; published 5 January 2009)

The structural, electronic, and phonon properties of Li_2O and Li_2CO_3 solids are investigated using density functional theory (DFT) and their thermodynamic properties for CO_2 absorption and desorption reactions are analyzed. The calculated bulk properties for both the ambient- and the high-pressure phases of Li_2O and Li_2CO_3 are in good agreement with available experimental measurements. The calculated band gap of the high-pressure phase of Li_2O (8.37 eV, indirect) is about 3 eV larger than the one corresponding to the ambient Li_2O phase (5.39 eV, direct), whereas the calculated band gap for the high-pressure phase of Li_2CO_3 (3.55 eV, indirect) is about 1.6 eV smaller than that for the ambient phase of Li_2CO_3 (5.10 eV, direct). The oxygen atoms in the ambient phase of the Li_2CO_3 crystal are not equivalent as reflected by two different sets of C-O bond lengths (1.28 and 1.31 Å) and they form two different groups. When Li_2CO_3 dissociates, one group of O forms Li_2O, while the other group of O forms CO_2. The calculated phonon dispersion and density of states for the ambient phases of Li_2O and Li_2CO_3 are in good agreement with experimental measurements and other available theoretical results. $Li_2O(s)+CO_2(g)\leftrightarrow Li_2CO_3(s)$ is the key reaction of lithium salt sorbents (such as lithium silicates and lithium zircornates) for CO_2 capture. The energy change and the chemical potential of this reaction have been calculated by combining DFT with lattice dynamics. Our results indicate that although pure Li_2O can absorb CO_2 efficiently, it is not a good solid sorbent for CO_2 capture because the reverse reaction, corresponding to Li_2CO_3 releasing CO_2, can only occur at very low CO_2 pressure and/or at very high temperature when Li_2CO_3 is in liquid phase.

DOI: 10.1103/PhysRevB.79.014301 PACS number(s): 61.50.Lt, 63.20.dk, 63.70.+h, 64.10.+h

I. INTRODUCTION

As solid electrolytes, lithium ceramics are widely used in high-energy lithium secondary batteries due to their high energies per unit weight and high lithium ion conductivity.[1,2] Lithium oxide (Li_2O, lithia) is the most basic lithium ceramic, and it is used as a thermal stabilizer for glasses. Having a low vapor pressure at high temperature, high tritium breeding capacity, high thermal conductivity, low electrical conductivity, and low tritium solubility,[3] lithium oxides are one of the best options for tritium production in the nuclear industry. Since lithia is one of the superionic materials, its diffusion and ionic conduction are subjects of interest. Both theoretical and experimental investigations have been performed on Li_2O to elucidate its energetic,[4–6] electronic[7–12] and defect properties,[13–15] ion conduction mechanisms,[15–17] and surface properties.[18]

Compared to the extensive investigations on its conductivities and tritium breeding capacities, there are few studies on lithia's CO_2 capture properties as a solid sorbent. Using thermogravimetric analysis, scanning electron microscopy, and x-ray-diffraction techniques, Mosqueda *et al.*[19] explored the behavior of Li_2O under an atmosphere of CO_2. Their results showed that Li_2O can be used for CO_2 retention through the reaction $Li_2O+CO_2\rightarrow Li_2CO_3$. CO_2 sorption depends on the diffusion of lithium through the formed shell of Li_2CO_3, with an extraordinary increase in the diffusion at 873 K. However, this study did not fully investigate the temperature and pressure dependence for the reverse reaction, $Li_2CO_3\rightarrow CO_2+Li_2O$, corresponding to releasing CO_2. While Li_2O is known to absorb CO_2 efficiently in the sorption reaction, a question remains as to whether Li_2CO_3 can release CO_2 easily in the desorption reaction under moderate temperature and/or pressure conditions.

In the past several years, there were many reports indicating that lithium silicates and lithium zirconates can be used as solid sorbents for CO_2 capture. Nakagawa and Ohashi[20] reported a novel method for capturing CO_2 from high-temperature gases through the reversible reaction $Li_4SiO_4+CO_2\leftrightarrow Li_2SiO_3+Li_2CO_3$ where Li_4SiO_4 maintains its absorption effectiveness during the cycle between absorption at 973 K and desorption at 1123 K in the presence of pure CO_2, at a total pressure of 1.0×10^5 Pa.[21,22] Venegas *et al.*[23] pointed out that the resultant Li_2SiO_3 produced from the initial CO_2 absorption could further react with CO_2, i.e., $Li_2SiO_3+CO_2\leftrightarrow SiO_2+Li_2CO_3$, making Li_4SiO_4 an even more efficient sorbent. Ochoa-Fernandez *et al.*[24] reported that CO_2 can be captured through the reaction $Li_2ZrO_3+CO_2\leftrightarrow ZrO_2+Li_2CO_3$. Kato *et al.*[21,25] compared the adsorption behavior of Li_4SiO_4 with that of Li_2ZrO_3. They found that at a temperature of 500 °C, in the presence of 20% $CO_2(g)$ at ambient pressure, the weight increase of Li_4SiO_4 was about 50% greater than that of Li_2ZrO_3. In addition, Li_4SiO_4 absorbed CO_2 more than 30 times faster than Li_2ZrO_3. Essaki *et al.*[22] proposed that during the first half cycle, i.e., when the solid sorbents (Li_4SiO_4 and Li_2ZrO_3) capture the CO_2, the Li_2O migrates to the surface where it reacts with CO_2 and forms Li_2CO_3. During the second half cycle corresponding to CO_2 release, Li_2CO_3 dissociates into CO_2 and Li_2O. Li_2O subsequently reacts with Li_2SiO_3 or ZrO_2 to reform Li_4SiO_4 or Li_2ZrO_3. Although the details of the specific reaction mechanism have not been proven, the

general reaction $Li_2O+CO_2 \leftrightarrow Li_2CO_3$ still plays a critical role in CO_2 capture by the Li_4SiO_4 and Li_2ZrO_3 sorbent systems. This suggests that in order to fully understand the mechanisms for CO_2 capture of these solid sorbents, specific details about the thermodynamics of the $Li_2O+CO_2 \leftrightarrow Li_2CO_3$ reaction need to be determined.

Although the antifluorite phase of Li_2O has been extensively investigated with both experimental and theoretical methods,[4,6–18,26–28] its high-pressure anticotunnite phase was rarely studied.[29–31] Recently, Kunc *et al.*[31] explored the structural phase transition of Li_2O from anticotunnite to Ni_2In-type structure above 100 GPa. In the literature, there are several studies focusing on the Li_2CO_3 molecules[32–36] and ions.[37] However, only few theoretical studies have focused on description of the electronic and structural properties of Li_2CO_3 in crystalline phase. Based on DFT, Fedorov and co-workers[38,39] calculated the band structure and optical functions of Li_2CO_3 in the monoclinic phase. They found that the electron transfer between the σ and π orbitals of the crystallographically nonequivalent oxygen atoms can occur in different ways and that the role of cations in the stabilization of the anion chains is due to electron-cloud overlap among the atoms. Bruno and Prencipe[40] investigated the structural properties of the bulk and the low-index surfaces [(001), $(\bar{1}01)$, and (110)] of Li_2CO_3 at the Hartree-Fock (HF) and DFT levels. Their results showed that the (001) surface of Li_2CO_3 is the least stable, while the (110) surface is the most stable. Li_2CO_3 can also exist in a nonquenchable hexagonal polymorphic form above 10 GPa as observed by Grzechnik *et al.*[41] To our knowledge, no theoretical study has been done to investigate the electronic properties of this new phase. Therefore, in order to fully understand the mechanism of Li_2O absorbing CO_2, it is necessary to investigate the bulk and the electronic properties of Li_2O and Li_2CO_3 with state-of-the-art theoretical methods.

In this study, density functional theory was applied to explore the lattice-dynamical and electronic properties of the ambient- and high-pressure phases of bulk Li_2O and Li_2CO_3. Next, the chemical potential change with temperature and pressure for the reaction $Li_2O+CO_2 \leftrightarrow Li_2CO_3$ was calculated. Based on these data, the energetic and thermodynamic properties of the solid sorbent, Li_2O, as a candidate for CO_2 capture were evaluated.

This paper is organized as follows: Sec. II briefly describes the theoretical methods employed. Section III presents the results of the electronic structures for these crystals and compares these results with other available experimental and theoretical studies. The phonon properties of Li_2O and Li_2CO_3 in both ambient- and high-pressure phases, and the thermodynamic properties of the CO_2 capture reaction $Li_2O+CO_2 \leftrightarrow Li_2CO_3$ are also presented in this section. Section IV contains a brief summary and conclusions.

II. THEORETICAL METHODS

A. Density functional theory approach

The calculations performed in this work were based on first-principles DFT with plane-wave basis sets and the pseudopotential approximation to describe the electron-ion interactions. The Vienna *Ab initio* Simulation Package (VASP) (Refs. 42 and 43) was employed in this study to calculate the electronic structures of lithia and lithium carbonate materials. In this study, all calculations were done using the projector augmented wave (PAW) pseudopotentials and the PW91 exchange-correlation functional. This computational level was shown to provide an accurate description of oxide systems.[44] Plane-wave basis sets were used with a kinetic energy cutoff of 500 eV and an augmentation charge cutoff of 605.4 eV. The *k*-point sampling grids of $n_1 \times n_2 \times n_3$, obtained using the Monkhorst-Pack method,[45] were used for these bulk calculations, where n_1, n_2, and n_3 were determined to be consistent to a spacing of about 0.028 $Å^{-1}$ along the axes of the reciprocal unit cells. The corresponding *k*-point sets we used in our calculations were $8\times8\times8$ and $4\times6\times4$ for the α and β phases of Li_2O and $5\times7\times6$ and $8\times8\times6$ for the α and β phases of Li_2CO_3. During calculations, all atoms in the cell were relaxed to the equilibrium configurations. For the high-pressure phase calculations, the volume and the atoms in the cell were relaxed subject to a Pulay stress (input parameter PStress in VASP) set to the experimentally measured pressure value. For the band-structure calculations, the symbols and coordinates of the high-symmetry points in the first Brillouin zone of the crystals are taken from the definitions of Bradley and Cracknell.[46]

B. Phonon calculations using the direct method

A useful thermodynamic description of the phase stability and transition behavior for crystalline materials can be found based on calculation of the phonon frequencies. Approaches for these *ab initio* calculations fall into two classes: the linear-response method,[47,48] in which the dynamical matrix is expressed in terms of the inverse dielectric matrix describing the response of the valence electron density to a periodic lattice perturbation, and the direct method,[49–51] in which the forces are calculated via the Hellmann-Feynman theorem. In this study, we employed the PHONON software package,[52] in which the direct method is applied following the formalism derived by Parlinski *et al.*[51] The dynamical matrix $\mathbf{D}(\mathbf{k})$ of the crystal is defined in the direct method as

$$D(\mathbf{k};\mu\nu) = \frac{1}{\sqrt{M_\mu M_\nu}} \sum_m \Phi(0,\mu;m,\nu)\exp\{-2\pi i\mathbf{k}\cdot[\mathbf{R}(0,\mu) - \mathbf{R}(m,\nu)]\}, \quad (1)$$

where M_μ and M_ν are masses of atoms μ and ν, $\mathbf{R}(0,\mu)$ and $\mathbf{R}(m,\nu)$ are the atomic positions and m runs over all atoms of the crystal, $\mathbf{k}$ is the wave vector in the first Brillouin zone, and $\Phi(0,\mu;m,\nu)$ is the force-constant matrix that can be fitted based on the forces generated by atomic displacements from equilibrium configuration.

The eigenvalues of Eq. (1) give the phonon frequencies $\omega^2(\mathbf{k},j)$ and the polarization vectors $\mathbf{e}(\mathbf{k},j)$:

$$\omega^2(\mathbf{k},j)\mathbf{e}(\mathbf{k},j) = D(\mathbf{k})\mathbf{e}(\mathbf{k},j), \quad (2)$$

where j is the mode index. The phonon density of states $g(\omega)$ describes the frequency distribution of the normal modes and can be evaluated using $\omega(\mathbf{k},j)$ and $\mathbf{e}(\mathbf{k},j)$ as

$$g(\omega) = \sum_{i,\mu} g_{i,\mu}(\omega) = \sum_{i,\mu} \left\{ \frac{1}{nd\Delta\omega} \sum_{k,j} |e_i(\mathbf{k},j;\mu)|^2 \delta_{\Delta\omega}[\omega - \omega(\mathbf{k},j)] \right\}, \quad (3)$$

where $g_{i,\mu}(\omega)$ is the partial phonon density of states (PPDOS) of the selected atom (μ) vibrating along selected Cartesian coordinate (i); $\mathbf{e}_i(\mathbf{k},j;\mu)$ is the ith Cartesian component of the polarization vector for μ particle; n is the number of sampling wave-vector points; d is the dimension of the dynamical matrix which corresponds to the number of degree of freedom in the cell, $\Delta\omega$ is the frequency interval; and the delta function $\delta_{\Delta\omega}$ is defined as

$$\delta_{\Delta\omega}(x) = \begin{cases} 1 & \text{if } -\frac{\Delta\omega}{2} < x < \frac{\Delta\omega}{2} \\ 0 & \text{otherwise.} \end{cases} \quad (4)$$

Within the harmonic approximation, the internal energy (E_{tot}), the entropy (S_{tot}), and the harmonic vibrational Helmholtz free energy F_{harm} of the primitive unit cell are defined as[53]

$$E_{\text{tot}} = \frac{1}{2} r \int_0^\infty g(\omega)(\hbar\omega)\coth\left(\frac{\hbar\omega}{2k_BT}\right) d\omega, \quad (5)$$

$$S_{\text{tot}} = rk_B \int_0^\infty g(\omega) \left\{ \left(\frac{\hbar\omega}{2k_BT}\right) \left[\coth\left(\frac{\hbar\omega}{2k_BT}\right) - 1 \right] - \ln[1 - e^{-\hbar\omega/2k_BT}] \right\} d\omega, \quad (6)$$

$$F_{\text{harm}} = rk_BT \int_0^\infty g(\omega) \ln\left[2 \sinh\left(\frac{\hbar\omega}{2k_BT}\right) \right] d\omega, \quad (7)$$

where r is the number of degree of freedom in the primitive unit cell. It can be seen that the zero-point energy (E_{ZP}) can be obtained from Eq. (5) by taking $T \to 0$,

$$E_{\text{ZP}} = \lim_{T\to 0}(E_{\text{tot}}). \quad (8)$$

In phonon calculations, a $2\times2\times2$ supercell was created from the optimized unit-cell structure that was calculated based on DFT. Structures with a displacement of 0.03 Å of nonequivalent atoms were generated from the $2\times2\times2$ supercell and DFT calculations were further performed to obtain the force on each atom due to the displacements. These forces were input into the PHONON package[52] to fit the force matrix $\Phi(0,\mu;m,\nu)$. By solving Eqs. (1) and (2), the phonon dispersions and densities were carried out. Based on these results, the partition function has been computed and Eqs. (5)–(7) were used to calculate the thermodynamic properties, such as the internal energy, the free energy, the entropy, and the heat capacity, at different temperatures. This combined *ab initio* DFT-phonon calculation methodology was applied for each crystalline system considered in this paper in order to obtain its phonon-derived dispersion and the thermodynamic properties. These data were then used to determine the thermodynamic properties for chemical reactions relevant to CO_2 sorption systems. Based on this method, we have investigated the CO_2 capture reaction by Li_2O, i.e., $Li_2O + CO_2 \leftrightarrow Li_2CO_3$, under different temperature and pressure conditions as presented in Sec. III E.

III. RESULTS AND DISCUSSIONS

A. Crystalline structures of Li_2O and Li_2CO_3

Lithium oxide (Li_2O) is one of the simplest ionic oxides. At ambient pressure and temperature, it usually has a cubic antifluorite structure with a_0=4.610 Å [α phase, space group $Fm\bar{3}m$ (No. 225)],[16,54] although another rhombohedral phase ($R\bar{3}mH$) (Ref. 55) was reported that is slightly deformed from and coexists with the cubic phase, with $\alpha = 90.16 \pm 0.13°$. The crystal structure of α-Li_2O, as shown in Fig. 1(a), consists of a primitive cubic array of Li^+ ions with spacing $a/2$ at sites $(\frac{1}{4},\frac{1}{4},\frac{1}{4})$, while the O^{2-} ions occupy alternating cube centers located at (0.0,0.0,0.0) sites. Recently, a structural phase transition in Li_2O has been predicted[30] and observed experimentally.[29] Using synchrotron angle-dispersive x-ray diffraction and Raman spectroscopy on samples of Li_2O pressurized in a diamond anvil cell, Lazicki *et al.*[29] observed a reversible phase change from cubic antifluorite α phase (space group: $Fm\bar{3}m$) to orthorhombic anticotunnite phase [β phase; space group: *Pnma* (No. 62)] at 50 ± 5 GPa and ambient temperature. The crystal structure of β-Li_2O [Fig. 1(b)] consists of chains of distorted tricapped-trigonal prisms of cations parallel to the b axis, where the O atom occupies the $(0.745,\frac{1}{4},0.6)$ site and the Li atoms occupy the $(0.883,\frac{1}{4},0.305)$ and $(0.305,\frac{1}{4},0.570)$ sites. The distance between Li and O ranges from 1.664 to 2.246 Å with an average of 1.89 Å. This observed β-Li_2O structure is different from the structure predicted by Cancarevic *et al.*[56] based on *ab initio* calculations that excluded the influence of the external pressure. They found an orthorhombic structure in the *Pmna* (No. 62) space group but with the lattice constants of $a=b=3.996$ Å and $c=5.636$ Å. Kunc *et al.*[31] predicted that the upper pressure limit for the stability of the β-Li_2O is 135 GPa at $T=0$ K. Above that pressure, the β-Li_2O would transform to the densely packed Ni_2In-type structure ($P6_3/mmc$, No. 194). The experimental lattice constants, atom fractional coordinates, and the number of formula units per unit cell for these two phases of Li_2O are listed in Table I. Obviously, in α-Li_2O the two Li atoms have the same coordination environments, whereas in β-Li_2O the coordination environments of Li atoms are different and they form two different groups.

Alkali carbonates are widely used as structural and engineering materials. At room temperature, lithium carbonate (Li_2CO_3), also known as zabuyelite,[57] has a monoclinic structure with space group $C2/c$ (No. 15).[57–60] Its crystal structure, as shown in Fig. 1(c), is composed of planar CO_3^{2-} anions and lithium atoms tetrahedrally coordinated to the oxygen atoms. The high-pressure crystal structure and symmetry of Li_2CO_3 are different from those at ambient condi-

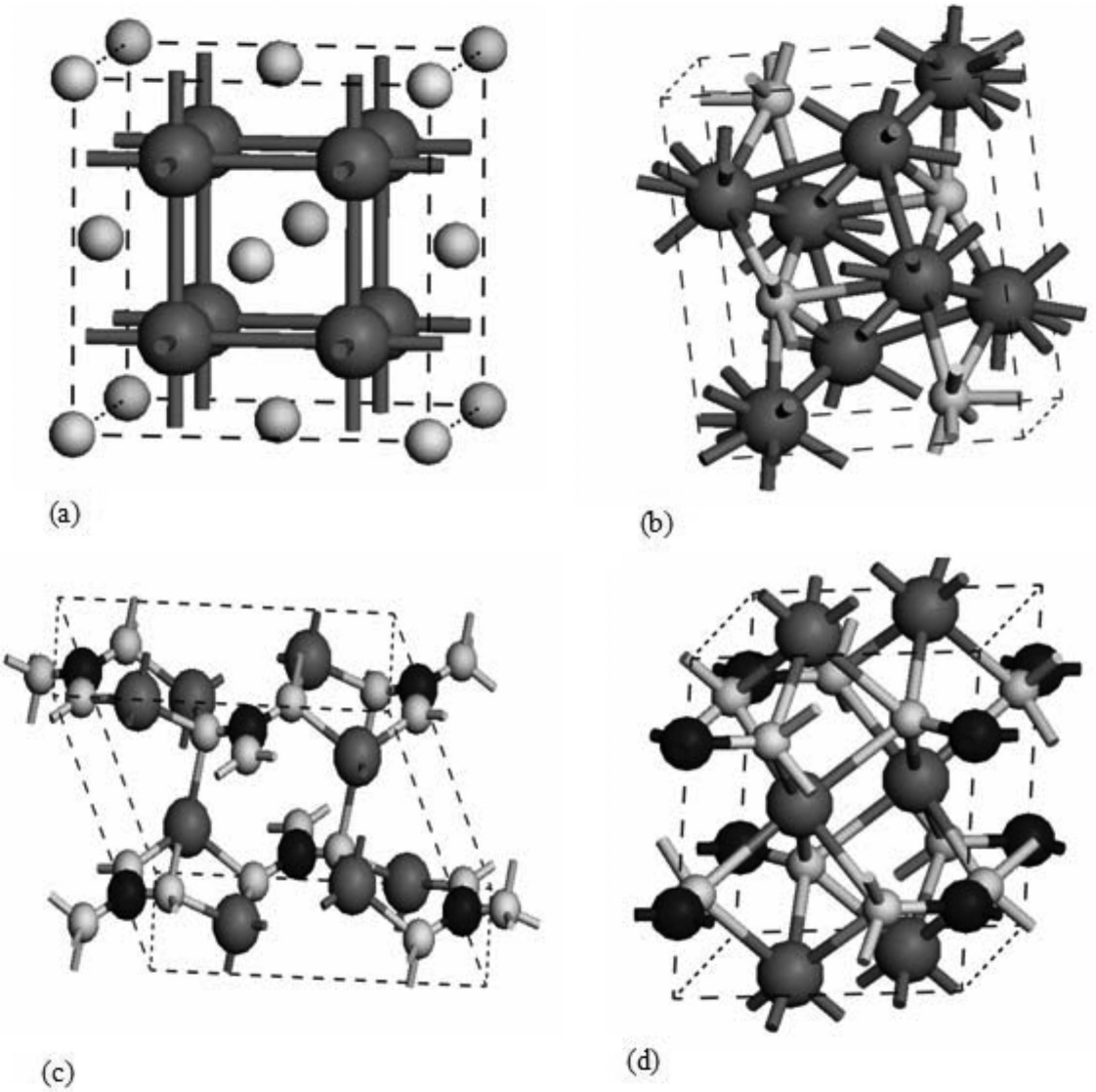

FIG. 1. The unit cells of Li_2O and Li_2CO_3 crystals. The biggest balls (in gray) stand for the Li atoms, middle-sized balls (in dark) stand for the C atoms, and smallest balls (in bright) stand for the O atoms. (a) The cubic antifluorite phase of Li_2O with $Z=4$ f.u., (b) the orthorhombic anticotunnite phase of Li_2O at pressure $P=62$ GPa with $Z=4$, (c) the monoclinic phase of Li_2CO_3 with $Z=4$, and (d) the hexagonal polymorph phase of Li_2CO_3 at $P=10$ GPa with $Z=2$.

tions. Using synchrotron angle-dispersive powder x-ray diffraction in diamond anvil cells and synthesis using a multianvil apparatus, Grzechnik *et al.*[41] found that a new nonquenchable hexagonal polymorph ($P6_3/mcm$, No. 193) occurs above 10 GPa where the carbonate groups are in a staggered configuration along the c axis [Fig. 1(d)]. The experimental lattice constants and the number of formula units per unit cell for these two phases of Li_2CO_3 are also listed in Table I. In this paper we refer to the ambient-pressure phase as the α phase and to the high-pressure phase as the β phase. From Figs. 1(c) and 1(d) and Table I, it can be seen that in the α-Li_2CO_3 crystal, the coordination environments of the O atoms are not the same and they can be divided into two groups, whereas in the β-Li_2CO_3 crystal, the coordination environments of O atoms are the same.

B. Structural optimization and bulk properties of Li_2O and Li_2CO_3

In order to explore the bulk properties of ambient- and high-pressure phases of Li_2O and Li_2CO_3, their total energies vs the changes in the cell volume were calculated and are shown in Figs. 2(a) and 2(b), respectively. Since each of the unit cells of Li_2O and the α-Li_2CO_3 contains 4 f.u., while the unit cell of β-Li_2CO_3 contains only 2 f.u. of Li_2CO_3, in Fig. 2 we plotted the relationship between energy and the unit-cell volume by normalizing to 1 f.u.

From Fig. 2 it can be seen that at ambient conditions the α phases of Li_2O and Li_2CO_3 crystals have lower energies compared to their corresponding high-pressure phases. When the pressure is increased (corresponding to decreasing the volume in Fig. 2), the β phases of Li_2O and Li_2CO_3 become

TABLE I. The experimental crystal structural parameters of Li_2O and Li_2CO_3 at ambient and high pressure.

Crystal		Lattice constants(Å)	Atom fractional coordinates	Space group	Formula unit Z
Li_2O	Antifluorite	a=4.610	O(0.0,0.0,0.0) Li($\frac{1}{4},\frac{1}{4},\frac{1}{4}$)	$Fm\bar{3}m$ (No. 225)[a,b]	4
	Anticotunnite (61.9GPa)	a=4.456 b=2.7865 c=5.212	O(0.745,$\frac{1}{4}$,0.6) Li(0.883,$\frac{1}{4}$,0.305) Li(0.305,$\frac{1}{4}$,0.570)	$Pnma$ (No. 62)[c]	4
Li_2CO_3	Monoclinic	a=8.358 84 b=4.973 75 c=6.193 77 β=114.789°	Li(0.1965,0.4484,0.8344) C(0.0,0.0657,$\frac{1}{4}$) O(0.0,0.32213,$\frac{1}{4}$) O(0.1459,0.0635,0.3127)	$C2/c$ (No. 15)[d,e]	4
	Hexagonal (10 GPa)	$a=b$=4.4568 c=5.1254 γ=120°	Li($\frac{1}{3},\frac{2}{3}$,0.0) C(0.0,0.0,$\frac{1}{4}$) O(0.2911,0.0,$\frac{1}{4}$)	$P6_3/mcm$ (No. 193)[f]	2

[a]Reference 16.
[b]Reference 54.
[c]Reference 29.
[d]Reference 58.
[e]Reference 59.
[f]Reference 41.

the stable phases. By fitting these data into the equation of state, the bulk properties of the crystals can be obtained. For this purpose we have used the Birch-Murnaghan equation of state in the (E,V) representation:[61,62]

$$E(V) = E_0 + \frac{9B_0V_0}{16}\left\{\left[\left(\frac{V_0}{V}\right)^{2/3} - 1\right]^3 B_0' + \left[\left(\frac{V_0}{V}\right)^{2/3} - 1\right]^2\left[6 - 4\left(\frac{V_0}{V}\right)^{2/3}\right]\right\}. \quad (9)$$

The fitted results [parameters E_0, V_0, B_0, and B_0' in Eq. (9)] of Li_2O and Li_2CO_3 are listed in Table II. The bulk modulus B is defined as $B=B_0+B_0'P$ in this scheme, where P is the pressure and set to 1 atm for ambient conditions. The cohesive energy (E_{coh}) is calculated by subtracting the total bulk energy at the minimum [E_0 in Table II and in Eq. (9)] from the sum of total energies of the isolated spin-polarized atoms (Li, O, and C) using the same level calculations (in our case, E_{Li}=−0.270 655 eV/atom, E_C=−1.212 547 eV/atom, and E_O=−1.491 391 eV/atom). The calculated E_{coh} as well as other values from different references are listed in Table II.

The experimental lattice constant for the antifluorite (α phase) Li_2O at room temperature, as shown in Table I, is 4.610 Å.[16,54] As shown in Table II the optimized crystal constant of the α-Li_2O is 4.632 Å, which is only 1.42% larger than the experimental value and quite close to other calculated values.[8,18] For the anticotunnite (β phase) Li_2O, where a Pulay stress was applied to simulate the experimental high-pressure condition (P=61.9 GPa), the optimized crystal constants given in Table II have less than 1% deviation from the experimental values. Similarly, very good agreement between predicated and experimental structural parameters is observed for β-Li_2CO_3 (see data in Table II).

From Table II, it can be seen that the fitted values of V_0 for β phases of Li_2O and Li_2CO_3 are significantly larger than the experimental measurements. This is due to the fact that V_0 parameters in Table II do not correspond to the experimental observed equilibrium volumes at high pressure but to the minima of the curves shown in Fig. 2, around the ambient pressure. A similar result was also obtained by Kunc *et al.*[30] We note however, that when we applied the Pulay stress to simulate the experimental high-pressure conditions, our predicted crystal constants (see values in Table II) of β phases of Li_2O and Li_2CO_3 are very close to the experimental values.

From Table II it can be seen that the calculated cohesive energies (E_{coh}) of Li_2O of 12.510 eV for the α phase and 12.245 eV for the β phase are very close to the experimental value of 12.24 eV.[63] But they have about 0.5 eV discrepancies with the atomization energy of Li_2O (11.96 eV) as obtained by Islam *et al.*[8]

The calculated bulk modulus of α-Li_2O (82.2 GPa) is very close to the experimental value of 81.8 GPa obtained by Hull *et al.*[54] and to the other calculated values which span from 79.6 to 105 GPa.[6,10,15,27,29,30,56] The calculated bulk modulus of β-Li_2O (65 GPa) is closer to the values of 78.6 and 80.8 GPa obtained by Kunc *et al.*[30,31] and to the values of 59.0 and 61.3 GPa determined for another high-pressure phase with Ni_2In symmetry type,[31] but quite far away from the experimental value of 188 GPa fitted by Lazicki *et al.*[29] A potential explanation for this large discrepancy between different sets of values is provided by Kunc *et al.*[31]

In the literature, we could find only a few relevant bulk property data for Li_2CO_3 that can be used to compare with our results. As listed in Table II, the optimized crystal structure of α-Li_2CO_3 calculated by Bruno and Prencipe[40] is very close to our reported values. By comparing the results for α-Li_2CO_3 with the results for β-Li_2CO_3 as shown in Table II,

TABLE II. The optimized equilibrium crystal structure and the deviations from the experimental measurements, the bulk modulus, the cohesive energy (E_{coh}), and the fitted parameters of Birch-Murnaghan equation of state for Li_2O and Li_2CO_3. The optimized structures of the high-pressure phases of Li_2O and Li_2CO_3 were obtained at the external experimental pressures as given in Table I.

Crystal		Optimized structures		E_0 (eV/cell)	B_0 (eV/Å^3)	B_0'	V_0 (Å^3)	Bulk modulus (GPa)	E_{coh} (eV)
		Lattice constants (Å) and deviations (%)	Atomic coordinates						
Li_2O	Antifluorite (α phase)	4.631 (1.3%) 4.56–4.64,[a] 4.62[b]	O(0.0,0.0,0.0) Li($\frac{1}{4},\frac{1}{4},\frac{1}{4}$)	−57.769	0.513	4.074 3.99[c] 3.51[d]	99.541 98.96[c] 96.96[d]	82.2 81.8(expt.)[e] 82.6[c]	12.510 12.24(expt.)[f] 11.96[a]
	Anticotunnite (β phase)	a=4.482 (0.6%) b=2.765 (−0.7%) c=5.253 (0.8%)	O(0.746 58,$\frac{1}{4}$,0.6077) Li(0.9773,$\frac{1}{4}$,0.3213) Li(0.3487,$\frac{1}{4}$,0.5748)	−56.709	0.406	4.290 4.0[d] 3.95[c]	96.805 64.72[d] 94.76[c]	65.0 78.6[c] 188[d]	12.245
Li_2CO_3	Monoclinic (α phase)	a=8.405 (0.6%) b=5.028 (1.0%) c=6.294 (1.7%) β=114.8° (0.6%) a=8.34242[g] b=4.98371[g] c=6.29431[g] β=114.16°[g]	Li(0.1972,0.4470,0.8352) C(0.0,0.0665,$\frac{1}{4}$) O(0.0,0.3222,$\frac{1}{4}$) O(0.1469,0.0635,0.3142)	−158.180	0.346	5.846	265.722 233.78[h]	55.5	33.317
	Hexagonal (β phase)	a=4.507 (1.1%) c=5.133 (0.2%) γ=120°	Li($\frac{1}{3},\frac{2}{3}$,0.0) C(0.0,0.0,$\frac{1}{4}$) O(0.2874,0.0,$\frac{1}{4}$)	−78.271	0.404	4.645	116.349 88.167[i]	64.7	33.907

[a]From Ref. 8.
[b]From Ref. 27.
[c]From Ref. 30.
[d]From Ref. 29.
[e]From Ref. 54.
[f]From Ref. 63.
[g]From Ref. 40.
[h]From Ref. 59.
[i]From Ref. 41.

it can be seen that the former has lower E_0, higher E_{coh}, and lower bulk modulus, which means that α-Li_2CO_3 is more stable than β-Li_2CO_3 phase that exists at higher pressure.[41]

C. Electronic structures of Li_2O and Li_2CO_3

1. Li_2O

The calculated band structures of the α and β phases of Li_2O are shown in Figs. 3(a) and 3(b). In the figure the smaller letters stand for the high-symmetrical points which are located at the center of two adjacent high-symmetrical points. From Fig. 3 it can be seen that for both phases of Li_2O, their band structures contain two valence bands (VBs): the first VB is located below Fermi level and has a wider width; the second VB is located at significant lower energies (about −15 eV below the Fermi level) and has a narrower width. As shown in Fig. 3(a), the conduction band (CB) of the α-Li_2O has a small gap at the **L** point. This was also observed by Albrecht *et al.*[9] based on DFT–local-density approximation (LDA) calculations. By comparing our band structure of α-Li_2O along the wave vector **L**-**Γ**-**X** direction in Fig. 3(a) with the one calculated by Eithiraj *et al.*[64] using linear muffin-tin orbital in its tight-binding representation (TB-LMTO), one can see that their shapes are very similar to each other and between the two VBs there is a large energy gap. Clearly, from Fig. 3 it can be seen that α-Li_2O has a direct band gap at **Γ** point with a value of 5.39 eV, while the β-Li_2O phase [at high pressure (61.9 GPa)] has an indirect band gap (from **Γ** to the middle of **Y** and **S** points) with a value of 8.37 eV. Interestingly, the calculated band gap of the high-pressure phase of Li_2O is about 3 eV larger than the corresponding ambient phase since the crystal structures of these two phases are quite different, as shown in Fig. 1 and Table I. As discussed in our previous work,[44] the DFT underestimates the excited-state energies and the calculated band gaps are usually smaller than the experimental measurements. There are several ways to correct the band-gap values, for example, by using the *GW* or GGA+U (or LDA+U) method or by employing a so-called scissors operation that simply shifts rigidly the unoccupied energy levels. For example, as summarized by Islam *et al.*[8] the experimentally measured band gaps of Li_2O ranges from 6.6 to 7.99 eV.[65] Using ten special **k** points, Albrecht *et al.*[9] evaluated the *GW* corrections for α-Li_2O and found that this opens the band gap at the **Γ** point by 2.1 eV. By considering this correction to our calculated band gap of α-Li_2O, we obtained a value of 7.49 eV, which is close to the recent experimentally measured value of 7.99 eV.[65] Therefore, in order to obtain more precise band-gap values from standard DFT calculations, further corrections, such as *GW*, are needed. In Table III we summarized our calculated band-structural re-

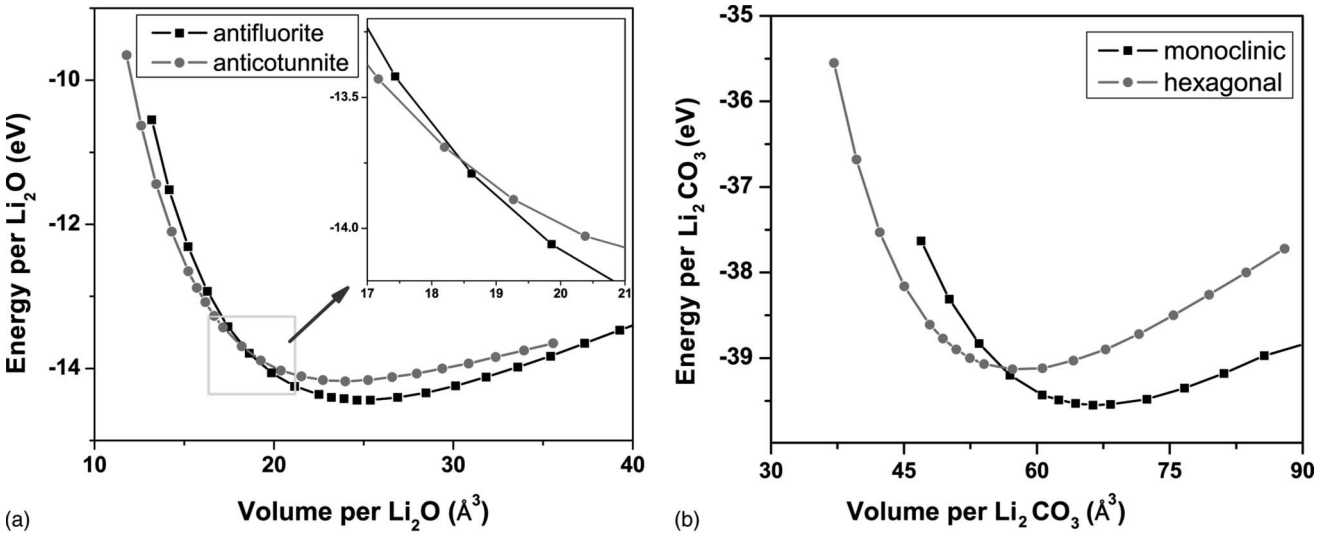

FIG. 2. The calculated total energy vs cell volume change for (a) Li_2O and (b) Li_2CO_3.

sults for both phases of Li_2O and compared them with the available literature data. We note however that the thermodynamic properties discussed later in this study related to CO_2 capture reaction are not dependent on the band-gap values.

As shown in Table II, by comparing the optimized fractional coordinates of the atoms with those from experimental measurements (Table I), one can see that in β-Li_2O the Li atoms have larger displacements along the a axis than along the b and c axes. From Fig. 1(a), one can see that in α-Li_2O each Li atom coordinates with four equivalent O atoms, while each O atom coordinates with eight equivalent Li atoms. The calculated Li-O bond length in α-Li_2O is 2.006 Å, which is quite close to the experimental value of 1.98 Å.[16,54] In β-Li_2O, as shown in Fig. 1(b), although the coordination environment of each O is the same, the coordination environments of Li atoms are not the same and can be divided into two groups [Li(I)-O and Li(II)-O] with nonequivalent Li-O bond lengths. The calculated bond lengths of Li(I)-O and Li(II)-O groups in β-Li_2O are 1.73, 1.73, 1.73, and 1.79 Å and 1.83, 1.90, 2.04, and 2.55 Å, respectively. These values are close to the experimental measurements of the polyhedral cation-anion distances ranging from 1.664 to 2.246 Å.[29]

The total density of states (TDOS) of Li_2O and the partial density of states (PDOS) of Li and O are shown in Fig. 4. From Fig. 4(b) it can be seen that the shape of PDOS of the two types (I and II) of Li atoms are slightly different because their coordination environments are not the same as described above. The p orbitals of Li(II) have a relatively larger contribution in the first VB compared with that of Li(I). By comparing the results in Fig. 4(a) with Fig. 4(b) and in Fig. 3(a) with Fig. 3(b), it can be seen that in both phases their second VBs are mainly from the s orbital of O, while their first VBs are from bonding of the p orbital of O with the s and p orbitals of Li. Interestingly, the p orbital of Li has a higher contribution in the upper portion of the first VB, compared with its s orbital. The conduction bands for both α and β phases of Li_2O are formed by both s and p orbitals of Li and O atoms.

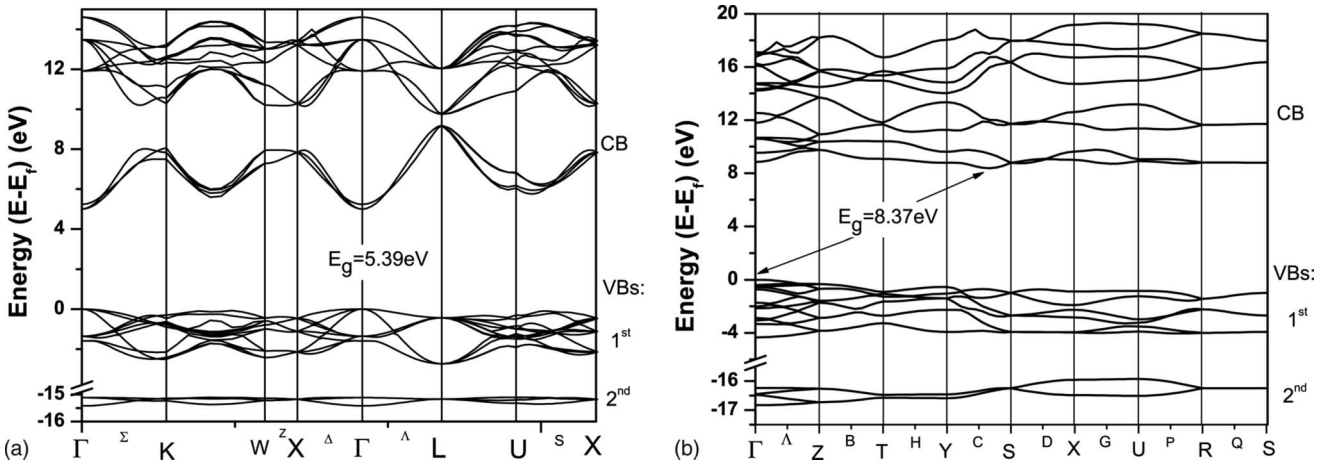

FIG. 3. The calculated band structures of Li_2O: (a) cubic antifluorite phase and (b) orthorhombic anticotunnite phase at P=61.9 GPa.

TABLE III. The calculated band gaps, valence-band widths, and zero-point energies (E_{ZP}) of Li_2O and Li_2CO_3 crystals (unit: eV).

Crystal		First VB width	Second VB width	Third and fourth VBs' widths	Band gap	E_{zp} (eV/f.u.)
Li_2O	α phase	2.59 2.0–2.7 [a] 1.402[c]	0.31		5.39 (direct) 7.49 (with GW)[b] 7.99 (expt.)[d] 7.4 (with GW)[e] 5.3,[e] 5.809[c]	0.23628
	β phase	3.95[c]	0.87		8.37 (indirect)	0.34991
Li_2CO_3	α phase	2.51 (0.53, 1.64)[f] 2.7[g]	3.49 (0.7, 1.99)[f] 1.0[g]	0.23, 0.35 0.22,[g,h] 0.42[h]	5.10 (direct) 5.0[g]	0.59912
	β phase	3.75	5.13	0.77, 1.15	3.55 (indirect)	0.61846

[a]From Ref. 11.
[b]The GW correction for α-Li_2O is 2.1 eV, taken from Ref. 9.
[c]From Ref. 10.
[d]From Ref. 65.
[e]From Ref. 9.
[f]There is a small gap within the first and second VBs of α-phase Li_2CO_3 as shown in Fig. 6(a). In parentheses are the bandwidths of these subbands.
[g]From Ref. 39.
[h]From Ref. 38.

2. Li_2CO_3

The calculated band structures of the α and β phases of Li_2CO_3 are shown in Figs. 5(a) and 5(b). From Fig. 5 one can see that for both phases of Li_2CO_3 there are two VBs (the third and fourth) which have very low energies (below −18 eV) and narrow bandwidths. These two VBs correspond to $3a_1'$ and $2e'$ valence orbitals with orbital energies below −20 eV, as demonstrated by x-ray spectroscopy.[37] As shown in Table III, the calculated bandwidths of the third and fourth VBs for α-Li_2CO_3 are close to the values calculated by Fedorov and co-workers.[38,39] In the case of monoclinic α phase of Li_2CO_3 shown in Fig. 5(a), within the energy range from

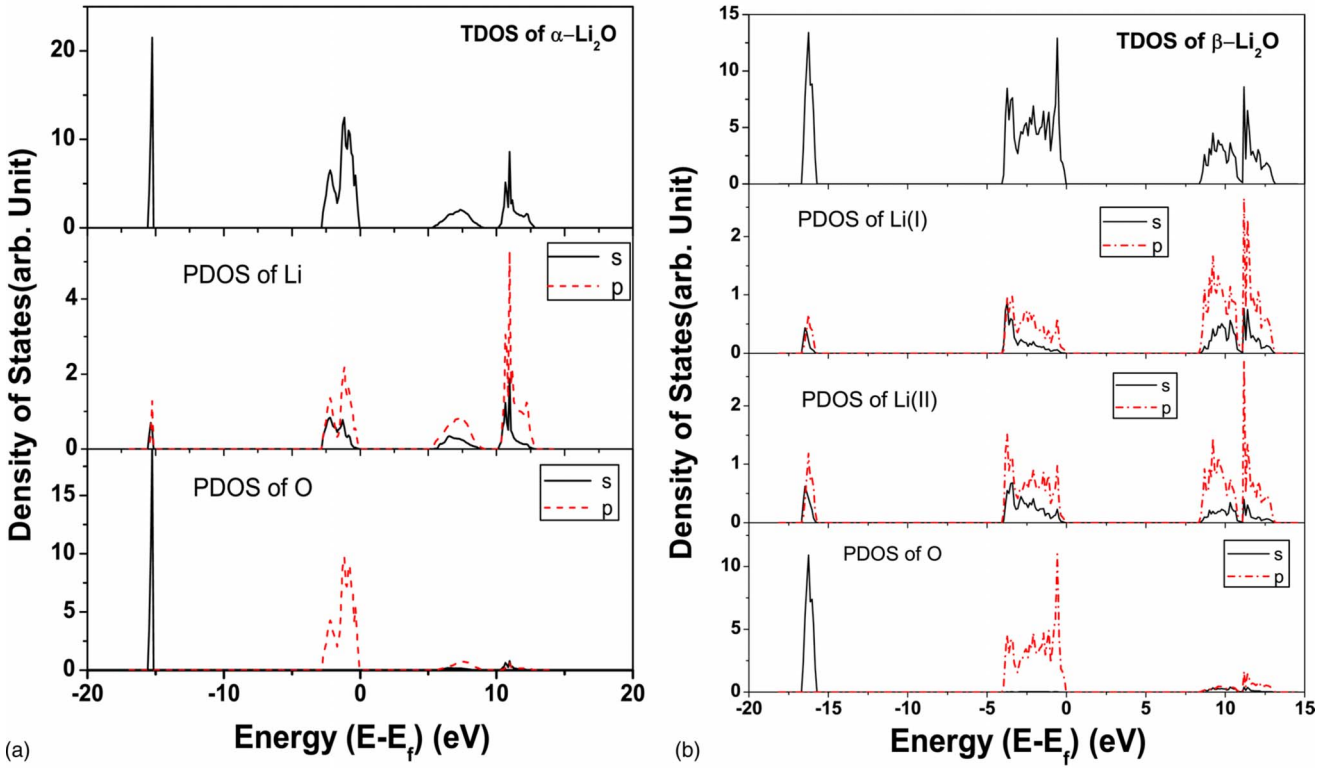

FIG. 4. (Color online) The calculated densities of states of Li_2O for (a) the cubic antifluorite phase and (b) the orthorhombic anticotunnite phase at P=61.9 GPa with two types of Li atoms in the unit cell.

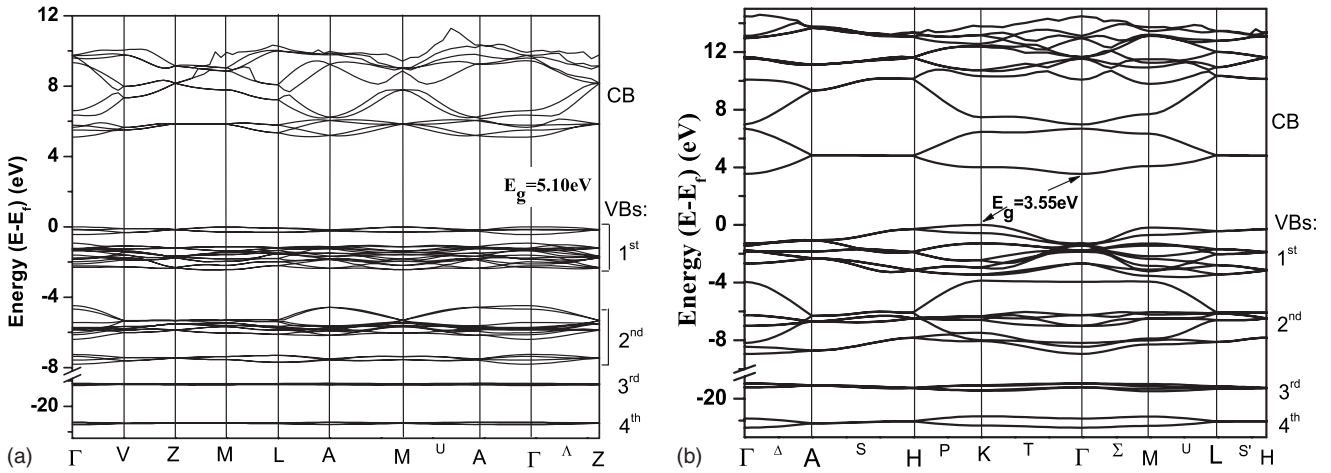

FIG. 5. The calculated band structures of Li_2CO_3: (a) monoclinic phase and (b) nonquenchable hexagonal polymorph at $P=10$ GPa.

−8 eV to the Fermi level E_F (set to relative zero), there are mainly two sets of VBs (hereafter denoted as the first and second). The corresponding widths are also listed in Table III. In Fig. 5(a) it can be seen that both the first and second VBs are split into two small VBs. Since the band gaps within these small VBs are quite small and in order to compare with the case of β-Li_2CO_3 readily, we treat them as two main VBs. As shown in Table III, the calculated bandwidth of the first VB for α-Li_2CO_3 is about 0.2 eV narrower than the values calculated by Fedorov and co-workers.[38,39] However, our calculated bandwidth of the second VB is much larger than their results.[38,39] In the case of the hexagonal polymorph (β phase) of Li_2CO_3 shown in Fig. 5(b), between the energy range from −8 eV to the Fermi level, only two VBs can be distinguished and the band gap between them is quite small. By comparing these two VBs with x-ray spectroscopy measurements,[37] it can be seen that they correspond to $3e'$, $1a_2''$, and $4a_1'$ valence orbitals. The calculated band gap of the α-Li_2CO_3 is a direct one at $\mathbf{\Gamma}$ point with a value of 5.10 eV. This value is very close to the one of 5.0 eV calculated by Zhuravlev and Fedorov.[39] In the case of β-Li_2CO_3 the band gap is an indirect one between the **K** and $\mathbf{\Gamma}$ high-symmetric points and has a value of 3.55 eV. Different from Li_2O, the calculated band gap of the high-pressure phase (β-Li_2CO_3) is smaller than that at ambient conditions (α-Li_2CO_3).

As shown in Table I and Fig. 1(c), in α-Li_2CO_3, the three C-O bonds are not equal: one bond length is 1.27 Å, while the other two bonds have the same length of 1.29 Å.[59] The Li-O bond lengths in α-Li_2CO_3 are 1.90 and 1.94 Å, whereas in α-Li_2O the bond length of Li-O is 1.98 Å.[16,59] The three calculated C-O bond lengths of α-Li_2CO_3 are 1.28, 1.31, and 1.31 Å, which means that these three O atoms can be divided into two groups O(I) and O(II) containing one and two O atoms, respectively. The O(I) also bonds with two Li atoms with the same bond length [O(I)-Li] of 1.91 Å, while O(II) bonds with three Li atoms with different bond lengths [O(II)-Li] of 1.97, 2.00, and 2.04 Å [see Fig. 1(c)]. These results are in good agreement with other experimental and theoretical findings.[32,40,57] However, in β-Li_2CO_3, due to the high symmetry of the crystal,[41] all three C-O bonds are the same and each O atom is also equivalently coordinated by four Li atoms as shown in Fig. 1(d). The calculated C-O and Li-O bond lengths are 1.29 and 2.04 Å, which are very close to the experimentally measured values of 1.298 and 2.0403 Å, respectively, determined by Grzechnik *et al.*[41]

Shown in Figs. 6(a) and 6(b) are the TDOSs of two phases of Li_2CO_3 and the PDOSs of Li, C, and O atoms. In order to address the different coordination environments around the O atoms in α-Li_2CO_3, shown in Fig. 6(a) also are the PDOSs of the two types of O (I and II) atoms, from which one can see that there are some differences between them. From Fig. 6 it can be seen that the third and fourth VBs are mainly from the *s* and *p* orbitals of O and C atoms. The contribution from Li is very small. The lowest VB (the fourth VB below −20 eV) is dominated by the *s* orbital of O and C. Interestingly, the second lowest VB (the third VB, between −20 and −18 eV) is dominated by the *s* orbital of O and the *p* orbitals of C in both phases. The x-ray spectroscopy results also indicated that the atomic components for the fourth VB are C 2*s* 19%, O 2*s* 70%, and O 2*p* 10%, and for the third VB are C 2*p* 13%, O 2*s* 83%, and O 2*p* 3%.[37] These observations are very close to our calculated PDOS as shown in Fig. 6. For both phases of Li_2CO_3, their second VBs are mainly from all the *s* and *p* orbitals of Li, C, and O atoms. Interestingly, the orbital of C does not contribute much to the first VB which is mainly formed from the *p* orbital of O and the *s* and *p* orbitals of Li. These results are also in good agreement with the x-ray spectroscopy findings for CO_3^{2-} where the atomic components for the first VB ($4e'$ valence orbital) is C 2*p* 3% and O 2*p* 97%.[37] These findings indicate that the C atom only binds with O atoms and the Li atoms are mainly interacting with O. This feature reveals that when the Li_2CO_3 is dissociated into Li_2O and CO_2, the energy costs are mainly for breaking one of the O-C bonds.

Comparing with their ambient phases as shown in Table II, the high-pressure phases of β-Li_2O and β-Li_2CO_3 have higher energies and are less stable. Here in this study, when we discuss the CO_2 capture reaction, we only focus on their ambient α phases. When Li_2CO_3 starts to dissociate, the bonds between Li and O(I) atoms will become stronger and form a new Li_2O phase by breaking the C-O(I) bond and transferring two electrons from CO_3^{2-} to Li-O. At the same

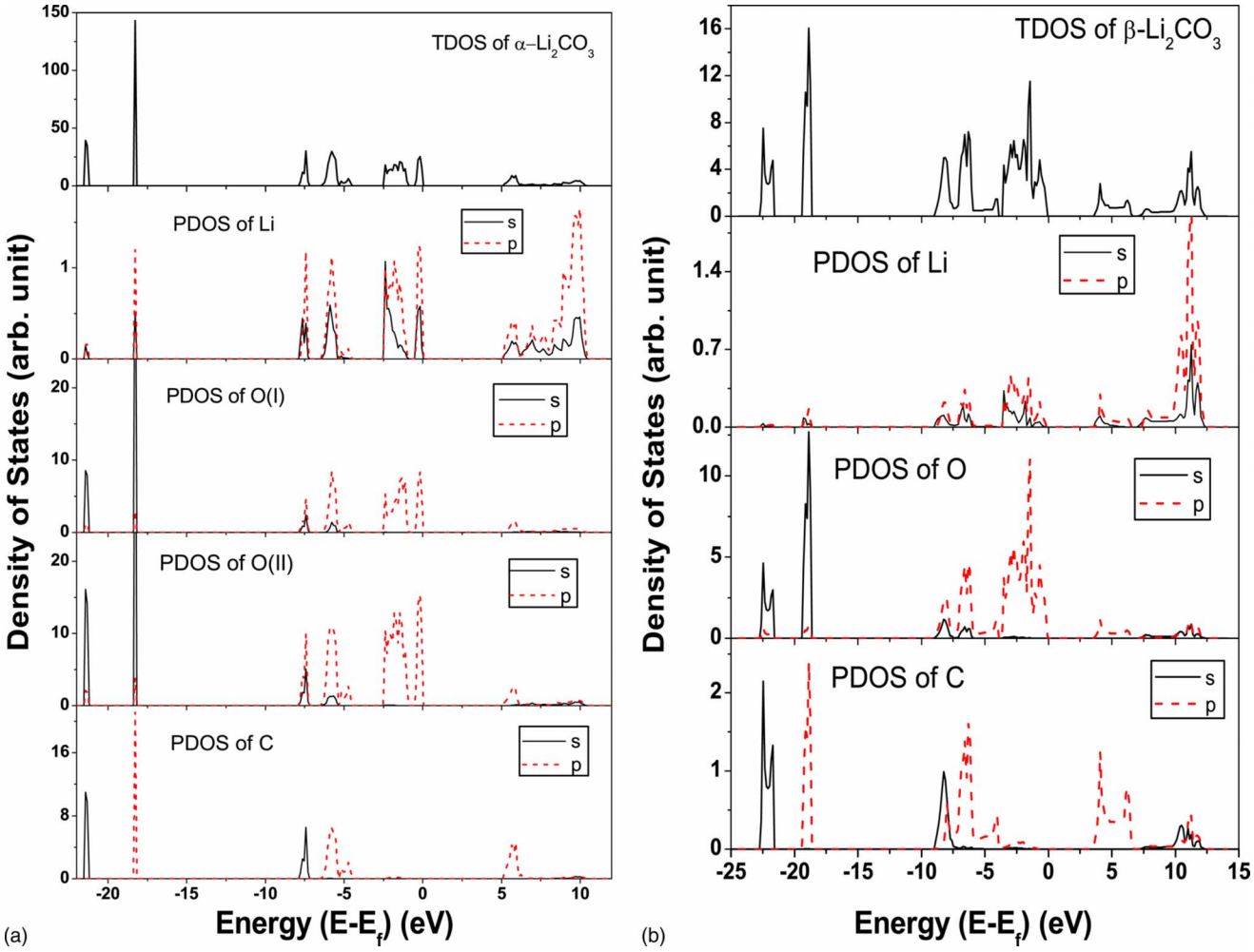

FIG. 6. (Color online) The calculated densities of states of Li_2CO_3 for (a) the monoclinic phase with two types of O atoms and (b) the nonquenchable hexagonal polymorph at $P=10$ GPa.

time, by losing one O, the CO_3 group will lead to formation of CO_2 molecule. For the direct reaction $Li_2O+CO_2 \rightarrow Li_2CO_3$, the CO_2 molecule will attack the O of Li_2O crystal and form a C-O bond as the crystal structure of Li_2O is transformed to Li_2CO_3. The detailed energetic analysis of this reaction will be discussed in Sec. III E.

D. Dynamical phonon properties of crystals Li_2O and Li_2CO_3

1. Li_2O

According to Eqs. (1) and (2), the calculated phonon dispersions of the two phases of Li_2O are shown in Figs. 7(a) and 7(b). Similar with the band-structure calculation as described in Sec. III C, the directions of the wave vectors in the first Brillouin zone follow the high-symmetric points as defined by Bradley and Cracknell.[46]

As we have indicated in Secs. III A and III C, different from its unit cell (Table I and Fig. 1), the α-Li_2O primitive cell contains 1 Li_2O f.u. Therefore it has nine branches of phonon modes as shown in Fig. 7(a). At $\mathbf{\Gamma}$ point, these nine branches are threefold degenerate and can be grouped into three sets. The lowest set is formed by three acoustical branches (T_{1u}): one longitudinal (LA) and two transverse (TA), which represent the motion of mass center and are infrared (IR) active. The other two sets are optical branches (T_{1u} and T_{2g}). The optical mode T_{1u} is infrared active and has a frequency of 12.855 THz (428.8 cm^{-1}). The Raman-active optical mode of T_{2g} symmetry occurs at 15.701 THz (523.73 cm^{-1}). Dovesi *et al.*[4] calculated frequencies of these two optical modes at HF level and obtained the values of 479 and 574 cm^{-1}, respectively. The experimental values of these two frequencies are 425 and 523 cm^{-1}, as measured by Osaka and Shindo.[66] Clearly, our results are much closer to the experimental measurements. By comparing our dispersion curve [Fig. 7(a)] with the results obtained by Farley *et al.*[67] for the **X**-**Γ**-**L** wave-vector range, it can be seen that the overall shapes and positions of the dispersion curves are similar to each other. The only difference is that in their report the threefold-degenerate optical modes (T_{1u}) at **Γ** point split into two sets (one- and twofold degenerate) due to the LO-TO splitting.[5,15,17] In order to determine the LO-TO splitting in this work, as an approximation, we replaced the effective charges in the PHONON program with the formal chemical charges and set the electronic dielectric constants to 1. We found that the infrared-active optical mode T_{1u} was

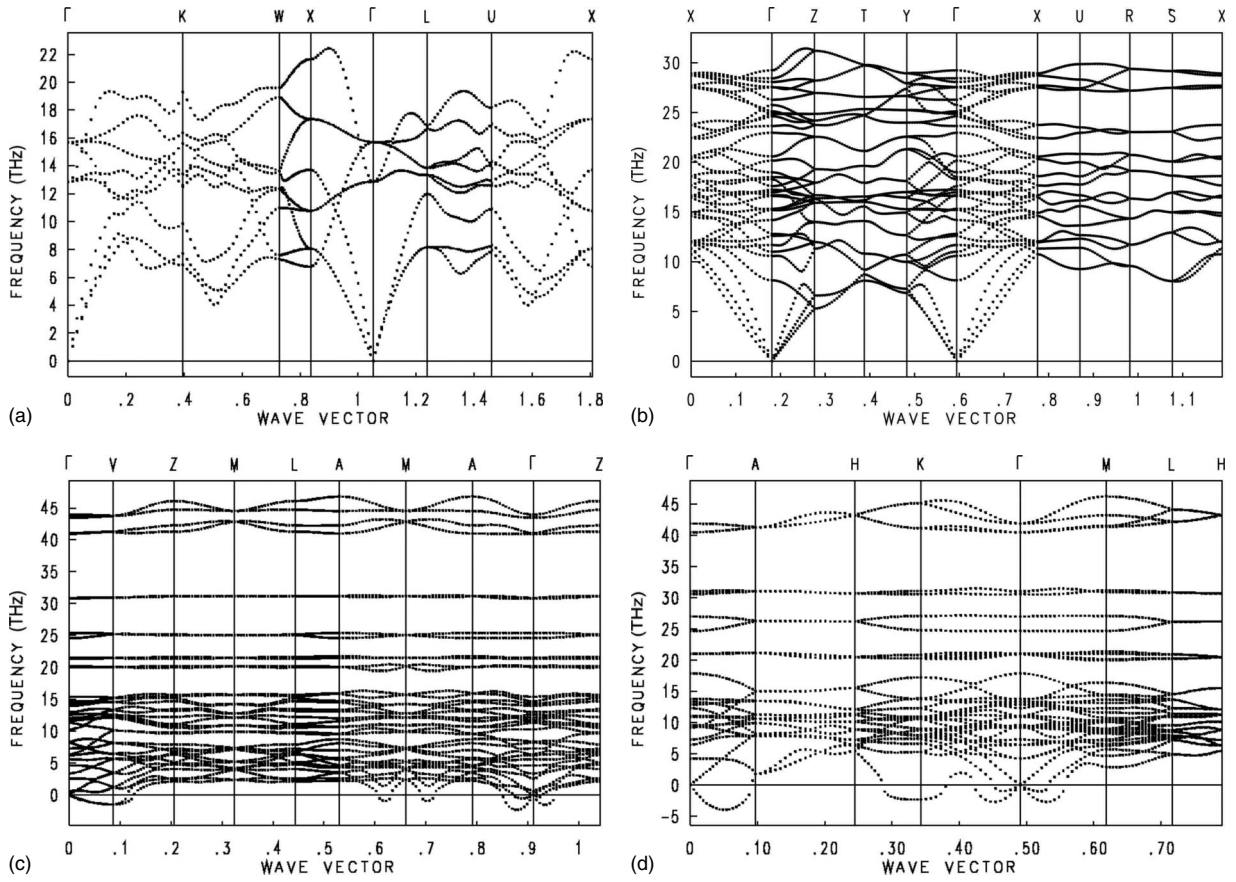

FIG. 7. The calculated phonon dispersions: (a) the cubic antifluorite phase of Li_2O, (b) the orthorhombic anticotunnite phase of Li_2O at $P=61.9$ GPa, (c) the monoclinic phase of Li_2CO_3, and (d) the nonquenchable hexagonal polymorph phase of Li_2CO_3 at $P=10$ GPa.

split into two sets: a twofold-degenerate mode with frequency of 12.86 THz (429.0 cm^{-1}) and a nondegenerate mode with a frequency of 33.44 THz (1115.4 cm^{-1}). These findings are fully consistent with the results obtained by Farley *et al.*[67] for α-Li_2O.

In the case of β-Li_2O high-pressure phase, there are four Li_2O units in its primitive cell, which results in 36 phonon branches as shown in Fig. 7(b). By comparing Fig. 7(b) with Fig. 7(a), it can be seen that for β-Li_2O at Γ point, all modes are nondegenerate. The reason is that this structure is under a pressure of 61.9 GPa, which produce stresses on each atom. The lowest frequency of the Raman-active optical mode (A_g) for β-Li_2O is 10.587 THz (353.2 cm^{-1}), which is lower than that of α-Li_2O (T_{2g}). At the present moment, there are no other phonon data for β-Li_2O which can be used for comparison to our calculated data.

Following Eq. (3), the calculated total phonon densities of states (TPDOSs) for α-Li_2O and β-Li_2O are presented in Figs. 8(a) and 8(b), respectively. For α-Li_2O, due to the high symmetry, the coordination environments for the two Li atoms are the same. From their PPDOSs, which are also shown in the bottom of Fig. 8(a), it can be seen that their PPDOSs along x, y, and z axes are almost the same. Similarly, the O atom also has a similar kind of symmetric PPDOS. As seen in Fig. 8(a), in this case, there are three groups of peaks. The middle one is from O atom vibration. The lower-frequency peak (5–10 THz) is determined by vibrations of both Li and O atoms, while the higher-frequency peak (14–20 THz) is mainly from Li atom. By comparing Fig. 8(a) with Fig. 8(b), it can be seen that the vibration frequencies span a larger range in the case of β-Li_2O because there are four Li_2O in its primitive cell which result in more vibrating modes. Among the frequency range from 0 to 22 THz, their TPDOSs are similar to each other. Due to the low symmetry in β-Li_2O, the two types of Li have different vibration modes. From the PPDOS of β-Li_2O (not shown in the figure), the higher-frequency (>22 THz) modes shown in Fig. 8(b) are from Li(I) atoms vibrating along x, y, and z directions. Among the observed modes those along x direction have lower vibrational frequencies than those along y and z directions. The second type of Li atoms [Li(II)] have contributions to the TPDOS in the range of 14–22 THz, while the O atoms contribute to the entire frequency range from 0 to 22 THz but they have relatively small amplitudes.

2. Li_2CO_3

In the cases of α-Li_2CO_3 and β-Li_2CO_3 one can see from Figs. 7(c) and 7(d) that the corresponding phonon-dispersion curves have some similarities: along the frequency axis, they are grouped into several bands just like their energy bands indicated in Figs. 5(a) and 5(b). These frequency bands do not vary much along the wave-vector axis. Within several regions, such as **Γ-V**, **M-A**, **Γ-A**, and **Γ-Z** in Fig. 7(c) for α-Li_2CO_3 and **Γ-A**, **K-H**, **Γ-K**, and **Γ-M** in Fig. 7(d) for

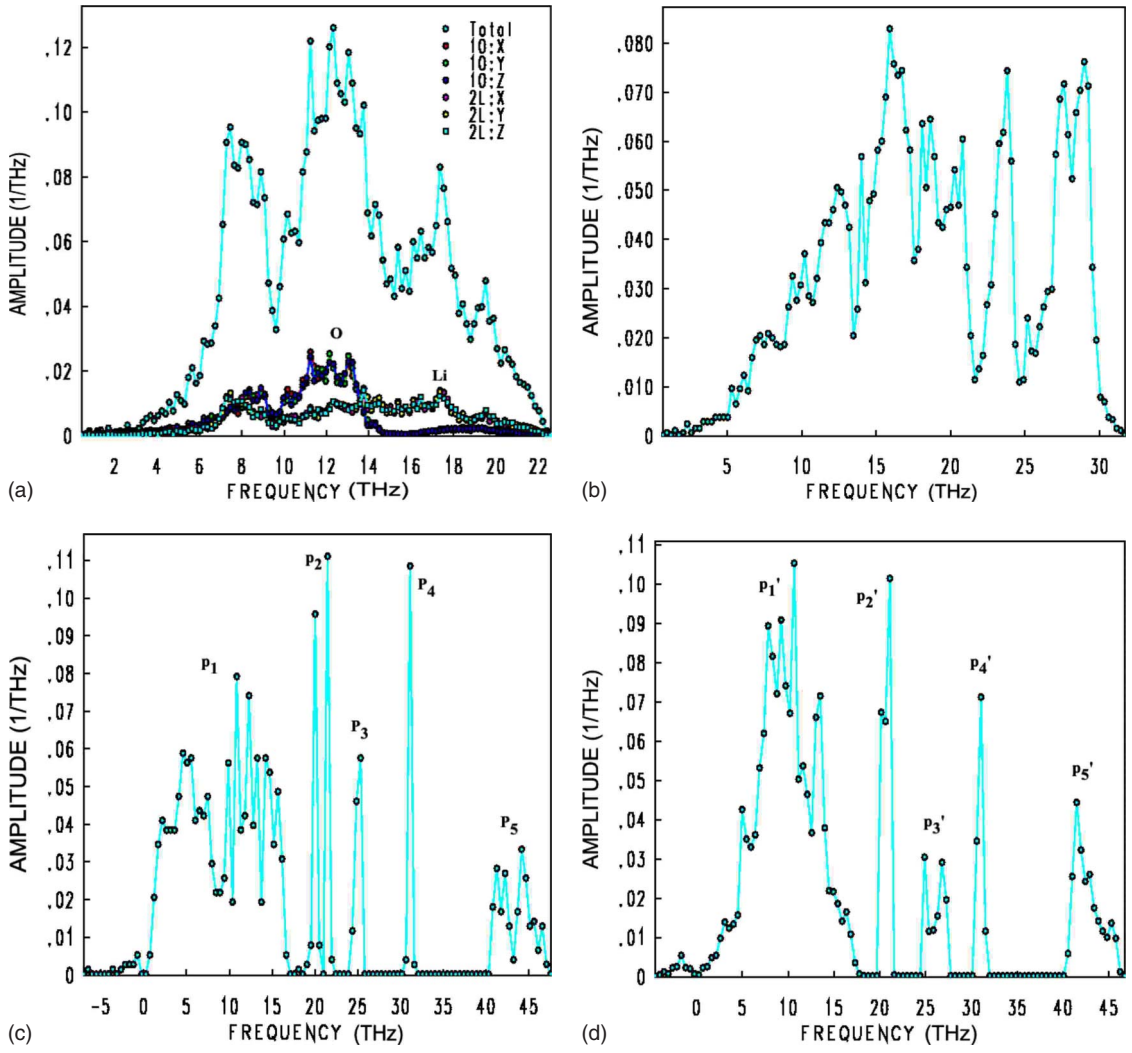

FIG. 8. (Color online) The calculated phonon total densities of states. (a) The cubic antifluorite phase of Li_2O. The partial densities of states of Li and O are also presented in the bottom portion. (b) The orthorhombic anticotunnite phase of Li_2O at $P=61.9$ GPa. (c) The monoclinic phase of Li_2CO_3. (d) The nonquenchable hexagonal polymorph phase of Li_2CO_3 at $P=10$ GPa.

β-Li_2CO_3, there are one or two soft modes (belonging to the acoustical branch) with imaginary frequencies and are shown as negative values in the figures. In the primitive cell of both α-Li_2CO_3 and β-Li_2CO_3, there are 2 Li_2CO_3 f.u. which result in 36 phonon branches as demonstrated in Figs. 7(c) and 7(d). Interestingly, in α-Li_2CO_3, all modes are nondegenerate (due to the crystal point group C_{2V}) and half of them are Raman active and half of them are infrared active. In β-Li_2CO_3, two-thirds of the vibration modes are twofold degenerate (E_g and E_u) and the others are nondegenerate (A_g, B_g, A_u, and B_u) due to its crystal point group D_{6h}. In the literature, there are several theoretically and experimentally measured Raman and IR spectra of α-Li_2CO_3, but no relevant data for β-Li_2CO_3 are available. In Table IV, we summarize our calculated phonon frequencies of α-Li_2CO_3 together with the corresponding irreducible representations and compare them with several other theoretical and experimental data.[35,68–73] From Table IV, it can be seen that overall our results are in good agreement with the available experimental and theoretical data, even if some small discrepancies can be noticed. A possible reason for the observed differences is that unlike other theoretical calculations,[73] in this work, except for setting the movement of mass center to zero frequency by applying translational-rotational invariance conditions, we did not further rescale our calculated data to fit the experimental measurements.

Shown in Figs. 8(c) and 8(d) are the TPDOSs of α-Li_2CO_3 and β-Li_2CO_3. It can be seen that the shapes of these two figures are similar and there are five peaks above 0 THz frequency, which correspond to the bands in Figs. 7(c) and 7(d). There is a very small peak below 0 THz in both crystals which comes from the soft modes. As discussed in Secs. III A and III C, the oxygen atoms in CO_3^{2-} planar group are divided into two groups: O(I) and O(II). Despite of bonding with C atom, the O(I) is bonded to two Li atoms, while O(II) is bonded to three Li atoms. When Li_2CO_3 is dissociated, these two O groups go to different products: $CO(II)_2$ and $Li_2O(I)$. From the PPDOS analysis (not shown in the figure), for α-Li_2CO_3 the lower portion of peak P_1 is dominated by the displacements of O(I) and O(II) along the x, y, and z directions and the displacement of C along z direction. The upper portion of peak P_1 is determined by the displace-

TABLE IV. The calculated and experimental measured vibrational frequencies of monoclinic (α-phase) Li_2CO_3 (unit: cm^{-1}). R stands for Raman-active modes and I stands for the infrared-active modes.

Irreducible representation vibration mode	Frequencies (cm^{-1})						
		Measured Raman and IR spectra			Calculated Raman spectrum		
	This work	Ref. 68	Refs. 69 and 70	Refs. 71 and 72	Ref. 35	Ref. 73	Ref. 68
A_u (I)	0						
B_u (I)	0						
B_u (I)	0						
B_g (R)	19.8						
A_g (R)	84.8	97	95				
B_u (I)	112.7			130[a]			
B_g (R)	154.2	128	126	134		167	164
B_g (R)	187.2	157	156	141		178	176
A_g (R)	207.8	194	192				
A_g (R)	212.9	219			211		
B_u (I)	243.8			220			
B_g (R)	274.3	274		254	232		
A_u (I)	278.4			277			
B_u (I)	343.0						
B_g (R)	378.6	380			353		386
A_u (I)	386.4		380				
B_u (I)	390.9		414	414			
A_g (R)	403.1			402		389	
A_u (I)	420.2		410	447			
B_g (R)	434.2	435		459	482	456	
A_u (I)	467.3		440	469			
B_u (I)	478.7		500				
A_g (R)	490.3	493		518	625	527	497
B_g (R)	514.3	518		547	635	581	575
A_u (I)	669.4			531			
A_g (R)	672.8		711		719	704	576
B_u (I)	712.4		713				
B_g (R)	717.7	714			741	721	716
B_u (I)	819.3		740[b]				
B_g (R)	846.6	747	748		892	873	776
A_g (R)	1003.4	1093	1091		1024	1041	1010
A_u (I)	1030.1		1088				
B_g (R)	1366.2	1411			1326	1323	1359
B_u (I)	1370.0		1420				
A_g (R)	1449.9	1460	1459[b]		1536	1482	1613
A_u (I)	1466.1						

[a]In Ref. 72, three other IR-active modes at 99, 160, and 196 cm^{-1} were reported.
[b]In Ref. 70, a very weak Raman-active mode at ~1720 cm^{-1} and two IR-active modes at 847 and 859 cm^{-1} were also reported.

ments of Li along x, y, and z directions and O(II) along z direction. P_2 has two peaks: the lower-frequency one is dominated by the displacements of O(II) along x direction and of O(I) along y direction, respectively, while the upper one is dominated by the displacements of O(II) along y direction and O(I) along x direction. P_3 is contributed from the displacement of C along z direction. P_4 is contributed from the displacement of O(I) along y direction and O(II) along x direction. P_5 also contains two peaks: the lower one is dominated by the displacement of C along x direction, while the upper part is contributed from the displacement of C along z direction. Similar conclusions can be drawn for the case of β-Li_2CO_3. However, in this case, the oxygen in CO_3^{2-} is indistinguishable due to its crystal symmetry. Peak P_1' is contributed by the displacements of O and Li atoms along x, y, and z directions, P_2' is dominated by the displacements of O

along x and y axes, P_3' is dominated by C atom displacement along z axis, while P_5' is dominated by the displacement of C along x and y axes. Similar to α-Li_2CO_3, peak P_4' is mainly contributed by the displacements of O along x and y directions.

From the PPDOS of each displaced atom and the polarization vector analysis, it can be found that these soft modes are from O displacements. For α-Li_2CO_3 as shown in Figs. 7(c) and 8(c), the soft modes between **Γ** and **V** are from displacements of O(II) along x, y, and z directions and O(I) along x direction. The soft mode between **M** and **A** (or **A** and **M**) is only from the displacement of O(II) along y direction. The upper soft mode between **Γ**-**A** and **Γ**-**Z** is from the displacements of O(I) and O(II) along z direction, whereas the lower soft mode is from the displacements of O(I) and O(II) along y direction. For β-Li_2CO_3 as shown in Figs. 7(d) and 8(d), the soft modes between **Γ**-**A** and **Γ**-**M** regions are from all the O displacements of CO_3^{2-} group as shown in Fig. 1 within xy plane, where the soft modes between **K**-**H**, **Γ**-**K**, and **Γ**-**M** are from one of O displacements from CO_3^{2-} group along z axis. These soft modes are related to distortion of the planar CO_3^{2-} group interacting with neighboring Li ions.

E. Thermodynamics of the reaction $Li_2O(s)+CO_2(g)\leftrightarrow Li_2CO_3(s)$

In practical applications as a CO_2 solid sorbent, Li_2O has a very high absorption weight percentage of 142.52% compared with other solid materials (such as Li_4SiO_4 with 36.72% and Li_2ZrO_3 with 28.78%).[20–25] As demonstrated by Mosqueda *et al.*,[19] Li_2O can absorb CO_2 to produce Li_2CO_3 up to 700 °C. When the temperature increases above 900 °C, dissociation of liquid Li_2CO_3 phase (its melting point is 710 °C) was found to take place, leading to rapid CO_2 release. These findings indicate that Li_2O is a good material for absorbing CO_2 but the optimal conditions for CO_2 release need to be investigated as well.

For the CO_2 capture reaction by Li_2O ($Li_2O+CO_2\rightarrow Li_2CO_3$), based on the results shown in Tables II and III, only the α phases of Li_2O and Li_2CO_3 need to be considered into this reaction because they are the stable phases at ambient-pressure conditions. We can ignore the PV contribution and assume that the difference between the chemical potential ($\Delta\mu^0$) of solid phases of α-Li_2O and α-Li_2CO_3 can be approximated by the difference in their electronic energy (ΔE^0) and the vibrational free energy of the phonons.[53] For CO_2, we can treat it as ideal gas. Therefore, the variation in the chemical potential ($\Delta\mu$) for this reaction with temperature and pressure can be defined as[44,74,75]

$$\Delta\mu(T,P)=\Delta\mu^0(T)-RT\ln P_{CO_2}, \tag{10}$$

with

$$\begin{aligned}\Delta\mu^0(T)&=\Delta E+\Delta E_{ZP}-(\Delta H-T\Delta S)_{gas}\\&\approx\Delta E^{DFT}+\Delta E_{ZP}+\Delta F_{harm}(T)-G_{CO_2},\end{aligned} \tag{11}$$

where ΔE_{ZP} is the zero-point energy difference between the reactants and products and can be obtained directly from phonon calculations using Eq. (8). ΔH and ΔS are the differences in enthalpies and entropies (vibrational, rotational, and translational parts) of CO_2 gas which contribute to the free energy of CO_2 (G_{CO_2}) and can be obtained by standard statistical mechanics,[76]

$$G_{CO_2}(T)\approx\frac{7}{2}RT+\sum_{i=1}^{4}\frac{N_A h\nu_i}{e^{h\nu_i/kT}-1}-TS_{CO_2}(T), \tag{12}$$

where N_A is the Avogadro constant. The entropy of CO_2 [$\mathbf{S}_{CO_2}(T)$] can be accurately evaluated using the Shomate equation.[77] The vibrational frequencies (ν_i) of CO_2 molecule are 673 cm^{-1} (π_u), 1354 cm^{-1} (σ_g^+), and 2397 cm^{-1} (σ_u^+),[78] from which the obtained zero-point energy for CO_2 molecule is 0.316 eV. Based on Eq. (8), the calculated zero-point energies (E_{ZP}) for Li_2O and Li_2CO_3 are listed in Table III. Therefore, the ΔE_{ZP} for this reaction is 0.04784 eV (or 4.62 kJ/mol). Based on phonon calculations under the harmonic approximation, the free energy of solids is described by the Helmholtz form F_{harm} given in Eq. (7). The energy of the CO_2 molecule is −22.994 089 eV as determined from calculations of an isolated molecule in a cubic box with the length of 20 Å. Overall, the DFT calculated energy change (ΔE^{DFT}, excluding ΔE_{ZP}) for the reaction $Li_2O+CO_2\rightarrow Li_2CO_3$ at $T=0$ K is −2.113 86 eV (−203.96 kJ/mol).

From Eqs. (11) and (12), it can be seen that the $\Delta\mu^0$ is temperature dependent because the ΔF and the free energy of CO_2 vary with temperature. The calculated free energies (F_{harm}) of α phases of Li_2O and Li_2CO_3 under different temperatures have been done according to Eq. (7) by ignoring the contributions of the soft modes in Li_2CO_3 with imaginary frequencies because these soft modes covered only a very small wave-vector space. As can be seen from Fig. 9(a) the phonon free energies of Li_2O and Li_2CO_3 decrease when the temperature increases. Around 600 K, they are close to each other and can be canceled out, resulting in $\Delta F_{harm}\rightarrow 0$ as given by Eq. (11). However, at both low ($T<400$ K) and high ($T>800$ K) temperatures, the differences between them become large. Usually the temperature range we are interested in is less than 1000 K because the melting point of Li_2CO_3 is 983 K.

Listed in Table V are the calculated free energies and the corresponding experimental values. For comparison, the results of the reactions for Li_4SiO_4 and Li_2ZrO_3 absorbing CO_2 are also listed in Table V. From this table, it can be seen that the free-energy change of Li_2O absorbing CO_2 is more negative than those for Li_4SiO_4 and Li_2ZrO_3, which indicates that Li_2O is better for absorbing CO_2 than the other two crystals.

By taking the activities of all phases of the reactant and product to be unity, the equilibrium pressure of the overall reaction can be calculated by setting $\Delta\mu(T,P)=0$ in Eq. (10), which leads to[79]

$$\frac{P}{P_0}=\exp\left(\frac{\Delta\mu^0(T)}{RT}\right). \tag{13}$$

By plotting the equilibrium pressures calculated from Eq. (13) as function of temperature T [see Fig. 9(b)] one can obtain the van't Hoff plot for CO_2 adsorption reaction by Li_2O.

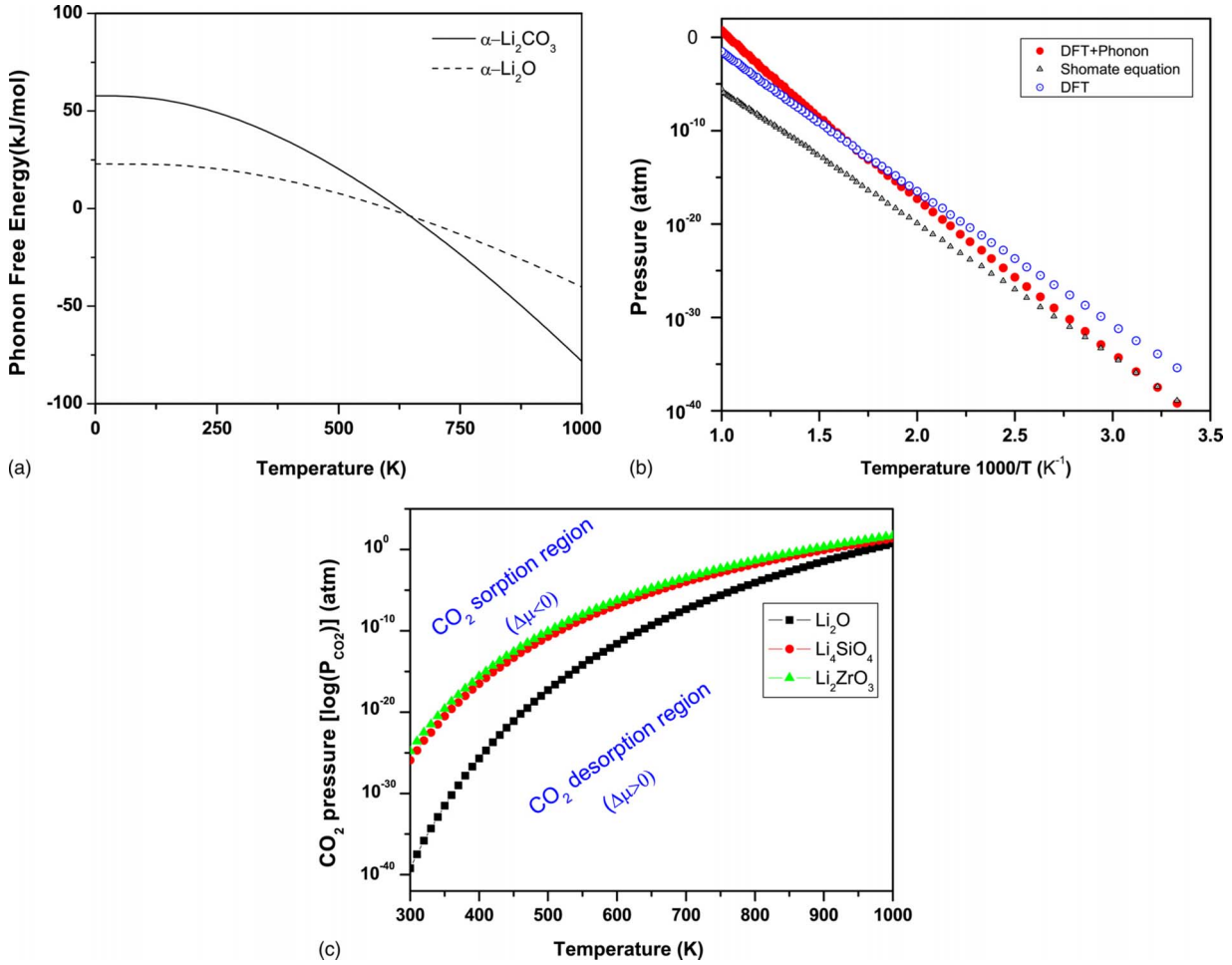

FIG. 9. (Color online) The calculated thermodynamic properties. (a) Phonon free energies of cubic antifluorite phase of Li_2O and monoclinic phase of Li_2CO_3. (b) van't Hoff plot for reaction $Li_2O+CO_2 \leftrightarrow Li_2CO_3$. The coefficients for Shomate equation are taken from Ref. 77. (c) The variation in the chemical potential $\Delta\mu$ with temperature and CO_2 pressure (P plotted in logarithmic scale) for the reaction of $Li_2O+CO_2 \leftrightarrow Li_2CO_3$. For comparison, data related to reactions $Li_4SiO_4+CO_2 \leftrightarrow Li_2SiO_3+Li_2CO_3$ and $Li_2ZrO_3+CO_2 \leftrightarrow Li_2CO_3+ZrO_2$ are also included. In each case the curve corresponds to the set of points for which $\Delta\mu=0$. Above the curve $\Delta\mu<0$ which means that the forward reaction is favorable to absorb CO_2, while below the curve $\Delta\mu>0$ which indicates that the reversed reaction to release CO_2 is favorable.

From Fig. 9(b) it can be seen that within the temperature range (300–1000 K) the equilibrium pressure is very low and increases with increasing the temperature. By including the phonon free energy and zero-point energy [Eq. (11)], the calculated P-T^{-1} curve is close to the one obtained based on Shomate equation for which the coefficients were fitted from experimental measurements.[77] The agreement between our calculated values and those obtained from experimental data is especially good in the range of 300–500 K. Overall, the curve calculated by DFT method which excludes the phonon free energy and zero-point energy (DFT only) is in poorer agreement with the Shomate equation than the one made by combining DFT and phonon (DFT+Phonon) data. We note however that the agreement level is temperature dependent and for temperatures larger than 820 K the DFT-only method provides better agreement than DFT+Phonon method as shown in Fig. 9(b).

From Fig. 9(b), in the temperature range (300–1000 K), it can be seen that the deviations of DFT-only results from the experimental measurements are almost constant. Therefore, the error introduced by ignoring the phonon free-energy contributions can be estimated. It has been proven[75,80] that the Gibbs free energies of solid phases have relatively small variations (<10 meV) in a wide range of temperatures (<1500 K) and pressures (<100 atm). Given the fact that the error levels determined by omission of the phonon contributions is small, as a first approximation we can neglect the zero-point energy change and the phonon free-energy change of the solids as shown in Eq. (11). This simplification allows a rapid screening of a large number of materials within a given database for variation in $\Delta\mu$ with temperature and pressure upon CO_2 capture reactions by eliminating the expensive computational time required by phonon calculations. After targeting out a small number of materials, further refinements of the DFT-only results can be considered by including the corresponding phonon data. This approach has been shown to be useful for predicting the thermodynamics of metal hydride systems.[79]

According to Eq. (10), we can explore the relationship among the chemical potential $[\Delta\mu(T,P)]$, the temperature,

TABLE V. The CO_2 weight percentages (wt %) and the calculated total-energy changes for CO_2 adsorption reactions by Li_2O, Li_4SiO_4, and Li_2ZrO_3 crystals. The pressure ranges (in atm) for the reverse reaction to release CO_2 at different temperatures is also indicated.

		Calculated free energy (kJ/mol)			CO_2 pressure range (atm) for $\Delta\mu \geq 0$ at different T (K)			
			$\Delta\mu^0(T=300\ \text{K})$					
Reaction	wt % CO_2	ΔE^{DFT}	(DFT+G_{CO2})	(DFT+Phonon+G_{CO2})	400 K	600 K	800 K	1000 K
$Li_2O+CO_2 \leftrightarrow Li_2CO_3$	142.52	−203.96	−203.55	−225.11	$<10^{-26}$	$<10^{-12}$	$<10^{-4}$	$<10^{-1}$
				−223.8[a]	(10^{-26}) [b]	(10^{-13}) [b]	(10^{-5}) [b]	(10^{-2}) [b]
				−326.35[c]				
$Li_4SiO_4+CO_2 \leftrightarrow Li_2SiO_3+Li_2CO_3$	36.72	−148.95	−148.54		$<10^{-16}$	$<10^{-7}$	$<10^{-2}$	$<10^{2}$
			−142.82[d]					
$Li_2ZrO_3+CO_2 \leftrightarrow ZrO_2+Li_2CO_3$	28.75	−142.61	−142.20		$<10^{-15}$	$<10^{-6}$	$<10^{-1}$	$<10^{2}$
			−160[e]					

[a]ΔH from Ref. 77 at $T=298$ K.
[b]For the case of DFT only.
[c]*Ab initio* calculation from Refs. 34 and 36.
[d]ΔH from Ref. 82 at $T=298$ K.
[e]ΔH from Ref. 83 at $T=298$ K.

and the CO_2 pressure (P_{CO_2}). In Fig. 9(c) this kind of relationship is shown for Li_2O sorbent system. The indicated curve in Fig. 9(c) corresponds to $\Delta\mu(T,P) \rightarrow 0$. Around this curve there is an optimal region for the absorption and desorption processes where the energetic requirements are minimal. Above this curve, the Li_2O is favorable to absorb CO_2 and to form Li_2CO_3, while below the curve the Li_2CO_3 is favorable to release CO_2 and to regenerate Li_2O. For comparison, in Fig. 9(c) we also included the calculated DFT data for two other sorbents: Li_4SiO_4 and Li_2ZrO_3.

As described above and shown in Fig. 9(c), the reaction of Li_2O with CO_2 with formation of Li_2CO_3 is thermodynamically favorable over a quite wide range of temperatures and P_{CO_2}. However, for practical applications, solid sorbents should not only absorb CO_2 efficiently but also should be optimized for CO_2 release. From Fig. 9(c) it can be seen that the reverse reaction to dissociate Li_2CO_3 and release CO_2 can only take place at very low P_{CO_2} ($<10^{-1}$ atm) and at very high temperature ($\sim$1000 K), where $\Delta\mu \geq 0$. These results agree well with experimental findings which also indicate that CO_2 release from Li_2CO_3 takes place only at high temperature and atmospheric pressure.[19] At low temperature, as demonstrated in Fig. 9(c) and Table V, Li_2CO_3 releasing CO_2 can take place only at very low CO_2 pressure (for example, $T=400$ K, $P_{CO_2} < 10^{-26}$ atm and $T=800$ K, $P_{CO2} < 10^{-4}$ atm). Comparing with Li_2O, the temperature and P_{CO_2} conditions for Li_4SiO_4 and Li_2ZrO_3 to capture CO_2 are moderate. As shown in Fig. 9(c) and Table V, it can be seen that Li_4SiO_4 and Li_2ZrO_3 can absorb CO_2 over a wide range of P_{CO_2} (10^{-25}–10^{2} atm) at moderate temperatures ($<$700 K). By increasing the temperature, the reverse reaction to release CO_2 happens over a wide P_{CO_2} range (10^{-25}–10^{-1} atm). These results are in quantitative agreement with the experimental findings.[20–25] However, in the case of Li_2O, our results indicate that this material is not a good solid sorbent candidate for capturing CO_2 because the release of CO_2 from Li_2CO_3 can only occur at very low pressures and/or at very high temperatures, which increase the operational costs. Listed in Table V are the CO_2-capturing conditions for Li_2O in comparison with those for Li_4SiO_4 and Li_2ZrO_3.

From Table V and Fig. 9(c) one can see that although the Li_2O has a higher CO_2 absorption weight percentage compared with the other two lithium salts (all of them absorb 1 mol of CO_2/mol of sorbent), the conditions for Li_2CO_3 to release CO_2 occur at higher temperatures and lower CO_2 pressures. Therefore, compared with Li_2O, the Li_4SiO_4 and Li_2ZrO_3 are better solid sorbent candidates for CO_2 capture because they can work at moderate temperatures and quite high CO_2 pressures. In the case of lithium silicate and zirconate, the reverse reaction involves not only dissociation of Li_2CO_3 but also the regeneration of Li_4SiO_4 and Li_2ZrO_3. This is done by reacting Li_2O with Li_2SiO_3 or ZrO_2 processes that involve a net energy gain. In turn, this leads to a less negative $\Delta\mu$. As a result, the presence of Li_2SiO_3 or ZrO_2 can destabilize the Li_2CO_3 phase and decrease the energy costs for the CO_2 release reaction. A similar destabilized behavior of Mg in the reaction of H_2 with Mg-Ni alloys was demonstrated by Reilly and Wiswall.[81] A more detailed analysis of the lithium silicate and zirconate solid sorbents is currently underway.

IV. SUMMARY AND CONCLUSIONS

In this study, the structural, electronic, and phonon properties of Li_2O and Li_2CO_3 solids in the ambient- and the high-pressure phases have been investigated by combining density functional theory and phonon calculations. We found that our results for their bulk properties, such as the bulk moduli, cohesive energies, optimized crystal constants, or phonon dispersion, are in good agreement with the available experimental measurements and other theoretical findings.

For these two solids, there are significant differences in the electronic properties between the ambient- and the high-pressure phases. The band structures of both the antifluorite (α) and anticotunnite (β) phases of Li_2O have two VBs.

Their first VBs are located just below the Fermi level and have widths of 2.59 and 3.95 eV, respectively. These bands are mainly from the interaction of the *p* orbital of O with the *s* and *p* orbitals of Li. The second VBs of the α and β phases are located below −15 eV and have narrow bandwidths of 0.31 and 0.87 eV, respectively. These bands are dominated by the *s* orbital of the O atoms. Interestingly, the band gap of high-pressure β-Li_2O (8.37 eV, indirect) is about 3 eV larger than the corresponding ambient-pressure α phase (5.39 eV, direct) due to different crystal structures. Due to the underestimation of the excited-state energies by standard DFT methods, the calculated band gaps usually are smaller than the experimental measurements. In order to improve the accuracy of the predicted band gap, further corrections, such as *GW* and LDA(or GGA)+U, are needed. By taking the *GW* correction into account, the calculated band gap of α-Li_2O (7.49 eV) was found to be close to the recent experimental measured value of 7.99 eV.[65]

The monoclinic phase (α) of Li_2CO_3 has four main VBs: the third and fourth VBs located below −18 eV are mainly from the *s* orbital of O and the *s* and *p* orbitals of C, while the first and second VBs located in the range from −10 eV to Fermi level are dominated by the interaction of the *p* orbital of O with the *s* and *p* orbitals of Li and C, respectively. Between the first and second VBs, there is a gap of about 2 eV. However, in the hexagonal high-pressure phase (β-Li_2CO_3), except for those two lowest-energy VBs (third and fourth), the first and second VBs located below the Fermi level are almost merged into one as the gap between them is only 0.14 eV. Different from Li_2O, the calculated band gap of β-Li_2CO_3 (3.55 eV, indirect) is about 1.5 eV smaller than that of α-Li_2CO_3 (5.10 eV, direct). Interestingly, in both phases of Li_2CO_3, the C does not contribute much to the first VB located just below the Fermi level and only interacts with the O to form a lower-energy band (second VB). The O atoms in α-Li_2CO_3 are nonequivalent and form two groups in which the O atoms are bonded to two and three Li atoms. When Li_2CO_3 starts to dissociate, one group of O interacts with Li atoms to form Li_2O and the other group of O interacts with C to form CO_2.

The phonon dispersions and phonon densities of states for both phases of Li_2O and Li_2CO_3 were calculated by the direct method. There are some significant differences between the phonon properties of the ambient phase and those of the high-pressure phase for both Li_2O and Li_2CO_3. The calculated vibrational frequencies are in good agreement with the available experimental measurements and other calculated results. For Li_2CO_3, there are two soft modes that originate from the displacements of the O atoms along and perpendicular to the CO_3^{2-} plane. Based on the phonon dispersion, the phonon free energy, the internal energy, and the entropy were evaluated within the harmonic approximation and have been used to analyze the chemical potential for the reaction of Li_2O capturing CO_2.

The thermodynamic properties of Li_2O capturing CO_2 have been analyzed with a combination of DFT and phonon calculations. The reaction $Li_2O(s)+CO_2(g)\leftrightarrow Li_2CO_3(s)$ is key to the ability of the lithium salt sorbents, such as lithium silicates and lithium zircornates, to capture CO_2. From the calculated energy change and the chemical potential for the reaction $Li_2O(s)+CO_2(g)\leftrightarrow Li_2CO_3(s)$, the results indicate that Li_2O readily absorbs CO_2 over a wide range of temperatures (up to 1000 K) and CO_2 pressures (from 10^{-20} to 10^3 atm). However, we found that the reverse reaction, $Li_2CO_3(s)\rightarrow Li_2O(s)+CO_2(g)$, to release CO_2, can only take place at very low CO_2 pressures ($<10^{-20}$ atm) and/or at high temperatures (around 1000 K). As a result pure Li_2O is not a good candidate for CO_2 capture, when compared with Li_4SiO_4 and Li_2ZrO_3.

ACKNOWLEDGMENTS

This work was performed in support of the National Energy Technology Laboratory's Office of Research and Development under Contract No. DE-AM26-04NT41817, subtask 41817.660.01.01. One of us (Y.D.) thanks J. K. Johnson, J. Steckel, R. Anderson, and B. Zhang for fruitful discussions and critical reading of the paper.

*Author to whom correspondence should be addressed.
FAX: 412-386-4542. yuhua.duan@netl.doe.gov

[1] M. A. K. L. Dissanayake and A. R. West, J. Mater. Chem. **1**, 1023 (1991).
[2] R. Collongues, A. Kahn, and D. Michel, Annu. Rev. Mater. Sci. **9**, 123 (1979).
[3] A. Donato, Fusion Eng. Des. **38**, 369 (1998).
[4] R. Dovesi, C. Roetti, C. Freyria-Fava, M. Prencipe, and V. R. Saunders, Chem. Phys. **156**, 11 (1991).
[5] P. Goel, N. Choudhury, and S. L. Chaplot, Pramana, J. Phys. **63**, 409 (2004).
[6] J. G. Rodeja, M. Meyer, and M. Hayoun, Modell. Simul. Mater. Sci. Eng. **9**, 81 (2001).
[7] L. Liu, V. E. Henrich, W. P. Ellis, and I. I. Shindo, Phys. Rev. B **54**, 2236 (1996).
[8] M. M. Islam, T. Bredow, and C. Minot, J. Phys. Chem. B **110**, 9413 (2006).
[9] S. Albrecht, G. Onida, and L. Reining, Phys. Rev. B **55**, 10278 (1997).
[10] R. D. Eithiraj, G. Jaiganesh, and G. Kalpana, Physica B **396**, 124 (2007).
[11] E. A. Mikajlo, K. L. Nixon, V. A. Coleman, and M. J. Ford, J. Phys.: Condens. Matter **14**, 3587 (2002).
[12] J. Viallon, M. A. Lebeault, F. Lepine, J. Chevaleyre, C. Jonin, A. R. Allouche, and M. Aubert-Frecon, Eur. Phys. J. D **33**, 405 (2005).
[13] N. Masaki, S. Nasu, T. Tanifuji, K. Uchida, K. Noda, H. Takeshita, T. Kurasawa, and H. Watanabe, J. Nucl. Mater. **116**, 345 (1983).
[14] K. Noda, K. Uchida, T. Tanifuji, and S. Nasu, Phys. Rev. B **24**, 3736 (1981).
[15] P. Goel, N. Choudhury, and S. L. Chaplot, Phys. Rev. B **70**,

174307 (2004).
[16] T. W. D. Farley, W. Hayes, S. Hull, M. T. Hutchings, and M. Vrtis, J. Phys.: Condens. Matter **3**, 4761 (1991).
[17] P. Goel, N. Choudhury, and S. L. Chaplot, J. Phys.: Condens. Matter **19**, 386239 (2007).
[18] A. Lichanot, M. Geilize, C. Larrieu, and C. Pisani, J. Phys. Chem. Solids **52**, 1155 (1991).
[19] H. A. Mosqueda, C. Vazquez, P. Bosch, and H. Pfeiffer, Chem. Mater. **18**, 2307 (2006).
[20] K. Nakagawa and T. Ohashi, Electrochemistry (Tokyo, Jpn.) **67**, 618 (1999).
[21] M. Kato and K. Nakagawa, J. Ceram. Soc. Jpn. **109**, 911 (2001).
[22] K. Essaki, K. Nakagawa, M. Kato, and H. Uemoto, J. Chem. Eng. Jpn. **37**, 772 (2004).
[23] M. J. Venegas, E. Fregaso-Israel, R. Escamilla, and H. Pfeiffer, Ind. Eng. Chem. Res. **46**, 2407 (2007).
[24] E. Ochoa-Fernandez, M. Ronning, T. Grande, and D. Chen, Chem. Mater. **18**, 6037 (2006).
[25] M. Kato, S. Yoshikawa, and K. Nakagawa, J. Mater. Sci. Lett. **21**, 485 (2002).
[26] A. Shluger, N. Itoh, and K. Noda, J. Phys.: Condens. Matter **3**, 9895 (1991).
[27] R. Dovesi, Solid State Commun. **54**, 183 (1985).
[28] K. Noda, K. Uchida, T. Tanifuji, and S. Nasu, J. Nucl. Mater. **91**, 234 (1980).
[29] A. Lazicki, C. S. Yoo, W. J. Evans, and W. E. Pickett, Phys. Rev. B **73**, 184120 (2006).
[30] K. Kunc, I. Loa, A. Grzechnik, and K. Syassen, Phys. Status Solidi B **242**, 1857 (2005).
[31] K. Kunc, I. Loa, and K. Syassen, Phys. Rev. B **77**, 094110 (2008).
[32] H. Morita, H. Ohata, K. Takeuchi, K. Ui, K. Kozawa, and N. Koura, Electrochemistry (Tokyo, Jpn.) **75**, 466 (2007).
[33] E. Herrera, F. Urena-Nunez, and A. D. Loya, Appl. Radiat. Isot. **63**, 241 (2005).
[34] V. G. Solomonik and I. S. Arychev, J. Struct. Chem. **32**, 183 (1991).
[35] F. Ramondo and L. Bencivenni, J. Mol. Struct. **221**, 169 (1990).
[36] S. P. Konovalov and V. G. Solomonik, J. Struct. Chem. **24**, 314 (1983).
[37] J. A. Connor, I. H. Hillier, and V. R. Saunders, Mol. Phys. **23**, 81 (1972).
[38] I. A. Fedorov, Y. N. Zhuravlev, and D. V. Korabel'nikov, Russ. Phys. J. **49**, 1106 (2006).
[39] Y. N. Zhuravlev and I. A. Fedorov, J. Struct. Chem. **47**, 206 (2006).
[40] M. Bruno and M. Prencipe, Surf. Sci. **601**, 3012 (2007).
[41] A. Grzechnik, P. Bouvier, and L. Farina, J. Solid State Chem. **173**, 13 (2003).
[42] G. Kresse and J. Hafner, Phys. Rev. B **47**, 558 (1993).
[43] G. Kresse and J. Furthmuller, Phys. Rev. B **54**, 11169 (1996).
[44] Y. Duan, Phys. Rev. B **77**, 045332 (2008).
[45] H. J. Monkhorst and J. D. Pack, Phys. Rev. B **13**, 5188 (1976).
[46] C. J. Bradley and A. P. Cracknell, *The Mathematical Theory of Symmetry in Solids* (Clarendon, Oxford, 1972).
[47] S. Baroni, P. Giannozzi, and A. Testa, Phys. Rev. Lett. **59**, 2662 (1987).
[48] S. Baroni, S. de Gironcoli, A. Dal Corso, and P. Giannozzi, Rev. Mod. Phys. **73**, 515 (2001).
[49] W. Frank, C. Elsasser, and M. Fahnle, Phys. Rev. Lett. **74**, 1791 (1995).
[50] K. Kunc and R. M. Martin, Phys. Rev. Lett. **48**, 406 (1982).
[51] K. Parlinski, Z-.Q. Li, and Y. Kawazoe, Phys. Rev. Lett. **78**, 4063 (1997).
[52] K. Parlinski, Software PHONON, 2006.
[53] M. Sternik and K. Parlinski, J. Chem. Phys. **123**, 204708 (2005).
[54] S. Hull, T. W. D. Farley, W. Hayes, and M. T. Hutchings, J. Nucl. Mater. **160**, 125 (1988).
[55] K. Masaki, K. Doi, S. Nasu, T. Tanifuji, and K. Uchida, J. Nucl. Mater. **84**, 341 (1979).
[56] Z. Cancarevic, J. C. Schon, and M. Jansen, Phys. Rev. B **73**, 224114 (2006).
[57] L. Pastero, F. R. Massaro, and D. Aquilano, Cryst. Growth Des. **7**, 2749 (2007).
[58] H. Effenberger and J. Zemann, Z. Kristallogr. **150**, 133 (1979).
[59] Y. Idemoto, J. W. Richardson, N. Koura, S. Kohara, and C. K. Loong, J. Phys. Chem. Solids **59**, 363 (1998).
[60] H. Ghobarkar and O. Schaf, Cryst. Res. Technol. **28**, 855 (1993).
[61] F. Birch, Phys. Rev. **71**, 809 (1947).
[62] F. D. Murnaghan, Am. J. Math. **59**, 235 (1937).
[63] A. Shukla, M. Dolg, P. Fulde, and H. Stoll, J. Chem. Phys. **108**, 8521 (1998).
[64] R. D. Eithiraj, G. Jaiganesh, G. Kalpana, and A. Rajagopalan, Phys. Status Solidi B **244**, 1337 (2007).
[65] Y. Ishii, J. Murakami, and M. Itoh, J. Phys. Soc. Jpn. **68**, 696 (1999).
[66] T. Osaka and I. Shindo, Solid State Commun. **51**, 421 (1984).
[67] T. W. D. Farley, W. Hayes, S. Hull, and R. Ward, Solid State Ionics **28-30**, 189 (1988).
[68] N. Koura, S. Kohara, K. Takeuchi, S. Takahashi, L. A. Curtiss, M. Grimsditch, and M. L. Saboungi, J. Mol. Struct. **382**, 163 (1996).
[69] J. B. Bates, M. H. Brooker, A. S. Quist, and G. E. Boyd, J. Phys. Chem. **76**, 1565 (1972).
[70] M. H. Brooker and J. B. Bates, J. Chem. Phys. **54**, 4788 (1971).
[71] H. Hase and I. V. P. Yoshida, Spectrochim. Acta, Part A **35**, 377 (1979).
[72] H. Hase and I. V. P. Yoshida, Spectrochim. Acta, Part A **35**, 379 (1979).
[73] F. Ramondo, L. Bencivenni, N. Sanna, and S. N. Cesaro, J. Mol. Struct.: THEOCHEM **253**, 121 (1992).
[74] S. Cristol, J. F. Paul, E. Payen, D. Bougeard, S. Clemendot, and F. Hutschka, J. Phys. Chem. B **106**, 5659 (2002).
[75] J. H. Wang and M. Liu, J. Power Sources **176**, 23 (2008).
[76] R. G. Mortimer, *Physical Chemistry* (Academic, New York, 2000).
[77] M. W. J. Chase, J. Phys. Chem. Ref. Data Monogr. **9**, 1 (1998).
[78] F. Gygi and G. Galli, Phys. Rev. B **52**, R2229 (1995).
[79] S. V. Alapati, J. K. Johnson, and D. S. Sholl, Phys. Chem. Chem. Phys. **9**, 1438 (2007).
[80] J. J. Xie, S. de Gironcoli, S. Baroni, and M. Scheffler, Phys. Rev. B **59**, 970 (1999).
[81] J. J. Reilly and R. H. Wiswall, Inorg. Chem. **7**, 2254 (1968).
[82] C. Gauer and W. Heschel, J. Mater. Sci. **41**, 2405 (2006).
[83] E. Ochoa-Fernandez, M. Ronning, X. Yu, T. Grande, and D. Chen, Ind. Eng. Chem. Res. **47**, 434 (2008).